

水力机械空化特性及控制策略研究

袁寿其

国家水泵及系统工程技术研究中心，江苏大学，镇江，212013

摘要：水力机械内部发生的空化是一种包含相变过程的复杂旋转湍流流动现象，空泡的发展、脉动、断裂以及溃灭所引起的流体动力是导致空蚀、振动和噪声，进而影响水力机械安全稳定运行的关键因素。针对水力机械的空化及其抑制问题，项目组经过多年的研究，发展了系统的空化流动实验技术，建立了水力机械内部非定常空化流动精确数值计算方法；揭示了非定常空穴形成和发展机理；掌握了空化发展与流体动力以及水力机械能量特性的关系；建立了水力机械的优化设计方法，提出了抑制水力机械空化的对策。

关键词：水力机械；空化；模型；非定常流动；可靠性

水力机械是关系国计民生以及国家安全的战略装备，作为重要的能量转换装置，水力机械广泛应用于国民经济的各个部门，空化问题一直是水力机械领域研究的关键核心问题，同时也是多种工程领域关键技术的核心问题，一直以来受到广泛的关注。项目组采用实验测试、机理研究、模型构建与模拟分析相结合的方法，对水力机械空化流动的测量，空化流动计算模型，空化初生和发展机理，空化动力特性及其机理，高空化性能水力机械模型开发，空化发展的抑制方法和机理等进行了深入研究。项目总体宏观技术路线如图1所示。

经过多年的研究，项目组建立了非定常空化多场实验测量平台和数据采集与处理系统，实现了非定常空化流场结构和压力脉动、振动噪声等参量的定量精确测量与同步分析；发展了适用于水力机械内部非定常空化流动的空化模型和湍流模型，建立了水力机械内部非定常空化流动数值计算方法。揭示了非定常空穴的形成和发展机理，特别是附着型空穴断裂及空泡脱落机制，掌握了空穴断裂、脉动和溃灭引起的冲击压强及其传播特性，以及不同空化阶段空化流激振动特性；掌握了关键几何参数对空化性能的影响，建立了空化性能预测模型，完善了高空化性能水力机械的优化设计方法，开发了高空化性能的水力模型。掌握了表面粗糙度和润湿性对空化初生和发展的影响以及主动通气对抑制空化及其诱导压脉动特性的影响机制，提出了泵类壳体及叶片微细裂纹激光强化延寿方法和激光诱导空泡空化强化方法，有效地抑制了水力机械的空化空蚀。项目研究成果已在舰船用泵和航空燃油泵得到应用，具有重要的理论意义和广阔的应用前景。具体成果主要如下：

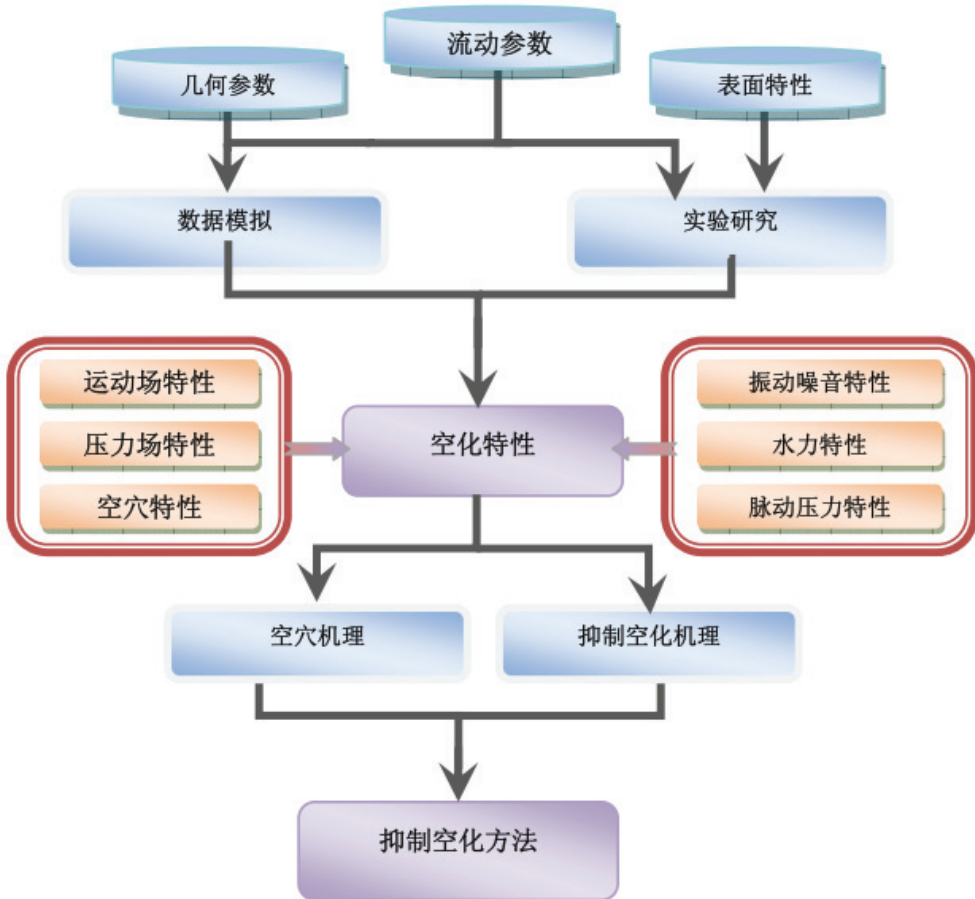


图 1 总体技术路线

1 非定常空化流动多场同步实验测量与分析技术研究

非定常空化流动现象涉及到空穴（空泡）形态、速度场和相分布等多场的相互作用，为研究各场的瞬态变化及相互间的关系，基于项目组现有的水洞、水力机械闭式试验台、实验仪器和设备，研究建立了多场测量实验平台，开发了数据采集和后处理分析系统。应用高速录像和高能量照明设备，发展了空化全流场实验技术，应用图像处理技术，开发了空化图像辨识、处理与分析系统，实现了对非定常空穴形态的捕捉与分析；并采用粒子图像测试技术获取了速度、涡量、湍流脉动等运动参数的分布及其变化特征，实现了空化非定常流场的测量与分析；基于流体动力学测量与分析系统，可测量空化水动力特性及特征频率。

2 水力机械非定常空化流动数值计算模型研究

考虑汽液混相的可压缩特性对湍流黏性系数的影响，应用一个密度函数代替混合密度，形成了一种基于密度的修正方式（Density corrected model, DCM）。引入密度修正函数后，在水蒸气含量较小的汽液混合区域，可以减小空化区域内的湍流黏性系数，从而减少湍流应力对空化流计算的影响，以期合理预测反向射流、空泡脱落等非定常流动行为。

离心泵的动静干涉及流道大曲率的结构特征，决定了离心泵内的流动极为复杂。项目组提出了考虑旋转效应与大曲率结构修正的改进方法。该方法在由 Spalart 在 Knight 和 Saffman 提出的回转稳态效应“gyroscopic stability effect”基础上建立，其基本思想是采用一个经验修正系数 $f_{rotation}$ 对湍流模型中的湍动能生成项进行修正，该修正方法代入 RNG $k-\varepsilon$ 湍流模型中，得到最终的 RCD 湍流模型。经对比分析发现 RCD 模型较好地捕捉到了附着空穴尾端空泡的脱落与溃灭现象，有效地解析出了空泡团的脱落和溃灭的过程，与试验结果吻合较好。

3 水力机械非定常空化湍流流场结构研究

以 Clark-Y 型水翼为研究对象，通过比较不同空化阶段流场结构，可以看出：空化现象对绕水翼的流场结构产生了显著的影响，水翼中后部的低速高涡量区对应于空化核心区域，空化的产生加剧了流场中的质量与速度交换，体现出更为明显的旋涡特性。利用粒子图像测速系统及相关软件，分析云状空化流场的速度、湍流脉动和涡量分布规律，及其与流场形态结构的相互关系。并与无空化流场结构进行对比，深入分析了云状空化湍流流场结构特性。

4 空化初生及发展机理研究

项目组对 Clark-Y 型水翼无分离流动条件下在初生空化阶段空化流随时间的演变过程进行了深入研究，发现初生空化在刚开始的阶段是以泡团的形式出现的，接着空泡串迅速增大并逐渐形成发夹型空化结构，随后开始了溃灭过程直至整个过程结束。结果表明，在现有雷诺数和翼型的几何条件下，相同结构发夹型空化结构不断地在相近的翼弦但不同的翼展位置产生随流而下，并重复着生成——长大——溃灭——反弹——再溃灭的相同过程。

利用数值计算和试验方法，以文丘里管和水翼为研究对象，深入地研究了不同空化发展阶段空穴形态演变规律、不同空化发展阶段空化诱导压力脉动变化规律、不同空化发展阶段时频特性变化规律、附着型空穴的非定常脉动及断裂特性及其流动机理以及大尺度脱

落空泡团的非定常特性。

5 离心泵不同空化阶段诱导振动噪声特性研究

在离心泵空化发展过程中，伴随着空泡的形成和溃灭，导致泵内不稳定流动，诱导产生非定常动力信号。空化的发生及空泡的溃灭会造成低频的压力振荡及高频的压力脉动，项目组以离心泵进出口压力脉动为例，分析泵空化的发展与泵进出口压力波动之间的关系。泵进口压力脉动的主频由轴频及其倍频组成，随着空化的发生发展主频存在明显的波动。受叶轮叶片与蜗壳隔舌动静干涉的影响，泵出口压力脉动主频由叶频与其谐波分量以及轴频与其谐波分量构成。振动信号可作为离心泵空化发生发展的特征信号，相对于流动诱导振动信号而言，空化诱导振动信号更为明显，强度更大。这说明离心泵因流量的变化所导致的流动不稳定对叶轮径向力的作用较弱，而泵内空化的发展可诱导产生强烈的激振力；与动静干涉相比，空化诱导振动信号占据主导作用。在空化诱导噪声方面，项目组通过对装置净正吸头逐渐降低过程中噪声信号的分析，建立离心泵空化的发展与声压信号之间的关系，获取离心泵空化初生点及不稳定空化发生点，探讨空化诱导噪声的特征信号。

6 离心泵关键几何参数对离心泵空化特性的影响

通过实验方法首次研究了叶片数、叶片进口冲角和叶片包角对离心泵设计流量下空化诱导振动和噪声特性的影响。研究结果表明随着其值下降，三种参数方案加速度传感器测得的振动强度均呈先基本保持不变再逐步上升的规律，且蜗壳第八断面测点上的振动强度最大叶片数、叶片进口冲角和叶片包角的变化对各测点的振动信号有明显影响，但变化规律较为复杂无空化发生时，三种参数的变化对噪声信号的轴频和叶频影响较大，且三种参数的变化规律不同，叶片包角的影响最为复杂。

7 基于神经网络的离心泵空化性能预测模型

采用改进算法的 BP 网络和径向基函数 (RBF) 网络来建立离心泵设计工况下的空化性能预测模型。根据空化的基本理论，选取影响泵空化余量的几个叶轮几何参数和设计点流量作为网络的输入变量，其中叶轮的几何参数包括：叶轮进口直径 D_1 、叶片进口宽度 b_1 、叶轮进口部分前盖板的曲率半径 R_1 、叶片进口冲角 $\Delta\beta$ 和叶片数 z 。确定 BP 网络和 RBF 网络的输入层神经元数目为 6，输出层神经元数目为 1，即为泵的必需空化余量。基于

MATLAB7.0 使用工具箱函数 newff 建立前向 BP 网络。将预测结果与实验值进行对比，BP 模型和 RBF 模型预测结果均具有较高预测精度，且 RBF 模型优于 BP 模型。

8 激光诱导空泡空化强化技术研究

研究激光技术对空泡的诱导和控制，利用激光空化强化技术提高泵部件的抗空蚀和耐腐蚀性能。研究激光强化对泵性能的影响，探讨激光强化与激光空泡空化产生的冲击波复合强化作用。研究表明，在保证结构强度的前提下，空化现象可以成为一种改善材料表面质量的有效手段。通过利用空化理论可以得到激光空泡射流的速度及对材料产生的压力，选择合适的激光参数，可实现水力机械激光空泡的空化强化；通过创新并巧妙地将原本对水力机械造成冲蚀破坏等副作用的空化空泡溃灭的高强度冲击力，转变为基体表面的高幅值残余应力，从而有效提高材料表面的微动疲劳抗力，从而改善材料的机械性能。

Research on cavitation characteristics and control strategies of hydraulic machineries

YUAN Shou-qi

National Research Center of Pumps, Jiangsu University, Zhenjiang, 212013

Abstract: Cavitation is a complex turbulent flow phenomenon including phase change that occurs in hydraulic machinery. The fluid dynamics caused by the development, oscillation, break up and collapse of the cavities are the main reasons that induce erosion, vibration and acoustic behavior of hydraulic machinery. These are the main factors that affect the reliability and safety of hydraulic machinery operations. Our project team has worked for many years, in order to investigate and control cavitation phenomena in hydraulic machinery. An experimental system for cavitating flow measurements has been developed. Furthermore, an accurate numerical method for the prediction of unsteady cavitating flow has been built to illustrate the mechanism of cavitation inception and development. The relationship between cavitation development, flow dynamics and energy characteristics of hydraulic machinery has been studied to achieve the best optimization method and control strategy for cavitation behavior in hydraulic machinery.

Key words: Hydraulic machinery; Cavitation; Model; Unsteady flow; Reliability

Unsteady cavitating flow around axisymmetric body at small angles of attack

LIU Hua

Department of Engineering Mechanics, Key Laboratory of Hydrodynamics(MOE), Shanghai Jiao Tong
University, Shanghai, China , Email: hliu@sjtu.edu.cn

Abstract: The presentation will focus on the unsteady cavitating flows and the hydrodynamic loads on an axisymmetric slender body at small angles of attack. A review on the unsteady behavior of cavitating flows, characterized as the cavity shedding at a specific range of cavitation number, around an axisymmetric body in the steady incoming flow or that in the steady translation motion will be presented. The periodic characteristics of unsteady cavitating flows around an axisymmetric body were investigated experimentally and numerically for the cases of different headforms and different angles of attack. The transient cavity shape and the transient hydrodynamic forces were measured by the high-speed camera and the five component balance respectively. The frequency characteristics of hydrodynamic forces and moment on axisymmetric bodies were obtained.

Based on the measured time series of drag and high speed image of cavity, an empirical formula was proposed to evaluate the Strouhal number of low frequency fluctuation of the violent shedding sheet cavitation for different headforms. The Strouhal number of the violent shedding of the unsteady cavitating flows around an axisymmetric body decreases as the angle of attack increases. The violent shedding will disappear as long as the angle of attack is greater than a critical value.

Numerical simulation of the unsteady flows around an axisymmetric body at angles of attack shows that a high pressure distribution on the body appears at the closure region of the cavity, where the detached sheet cavitation evolves to the cloud cavitation. Given the cavitation number, the shedding process of the cavitating flow is dependent of the headform and the angle of attack of the axisymmetric body.

For the case of the accelerating/decelerating incoming flows, an experiment on the unsteady hydrodynamic loads on a cavitating axisymmetric headform was implemented in a cavitation tunnel. The relationship between the hydrodynamic coefficients and the transient cavitation number was analyzed to understand the variation of the unsteady hydrodynamic loads with the

changes of the acceleration of incoming flows. Further discussion on the unsteady hydrodynamic loads on a ventilated supercavitating body in unsteady motion will be presented.

Finally, a review on the achievements of cavitation research made by Professor Yousheng He and his students at SJTU will be presented, covering hydrodynamic loads acting on a cavitating body in unsteady motion and on a body running with a cavity for water entry problems.

Uncertainty quantification for turbulent flow simulations: state-of-the art, challenges and open issues

XU Hui

(Department of Aeronautics, Imperial College London, London SW7 2AZ, United Kingdom,
Email: hui.xu@imperial.ac.uk)

Abstract: With the huge growth in high-performance computational resources, in order to remarkably prompt the contribution of turbulent flow simulation in real-life computational fluid dynamics (CFD) applications, it is important to quantify epistemic uncertainty in implementing simulations in terms of using Reynolds-Averaged Numerical Simulations (RANS), Large-Eddy Simulation (LES), hybrid RANS/LES and Direct Numerical Simulations (DNS) in many complex fluid flows. In CFD simulations, it is common that a large number of choices in setting up computational configurations should be made to mimic the real-life flow physics, which include the physical models and related arbitrary constants, boundary conditions, initial conditions as well as tunable parameters in employed numerical methods. In most cases, it is impossible to exactly known all physics and geometrical and sometime, these are even not known at all. These issues inevitably result in existence of uncertainties in complex turbulent flow simulations. To account for this lack of information in simulations, uncertainties in related models must be handled. This is the purpose of Uncertainty Quantification (UQ) theory, which allows for a quantitative description of the system response spanned by possible variation of uncertain parameters. The classical deterministic solutions are replaced by stochastic ones where a continuous description of the space of possible solutions spanned by uncertain parameters is recovered. Meanwhile, by virtue of the process of UQ, some possible new insights about the physics of the simulated system can also be achieved. The epistemic uncertainty can be reduced by incorporating existing data from experiments into the simulation, thanks to Data Assimilation (DA) techniques. In this talk, we provide a survey of recent progress made in the field of uncertainty and error quantification and propagation in turbulent flow simulations. All issues addressed are relevant to four fundamental methodologies: RANS, LES, hybrid RANS/LES and DNS. Finally, the talk concludes with challenges and open issues of UQ in turbulent flow simulations.

Key words: turbulent flow simulation; uncertainty quantification; generalized polynomial chaos; transitional flows

Brief introduction

Numerical modelling and simulation of complex systems which are generally governed by partial differential equations (PDEs) or ordinary differential equations (ODEs), are continuously developing in science and engineering. However, processes of modelling and simulation inherently involve deviations or errors from real physics systems, understanding and qualification of which are crucial to assess real behaviours of real physical systems. Typically, in modelling a real physical system described by partial differential equations, when a suitable mathematical model is formulated, the corresponding simulation always involve three steps ^[1]: case specification (geometry, boundary conditions, initial conditions, forcing, physical constants, model constants); simulation (numerical parameters, discretization resolution); analysis (solution, postprocessing). With these three steps, by simulation methods, real physics may not be always achieved in practice due to uncertainty of specified input data, numerical schemes, mathematical modelling and some intrinsic variabilities. Consequently, one must associate with simulations an uncertainty of incomplete knowledge from various possible factors. Theories and techniques for qualification and propagation of uncertainty have been well established for many years ^[1,2]. It is worth mentioning that spectral uncertainty quantification methods have broadly applied to deal with uncertainty, which are based on a parameterisation of uncertain input data employing a set of independent random variables. Generally, uncertainty quantification (UQ) is a two-stage process to cope with inverse / forward problems ^[1,4]. An inverse problem is to use experimental data to infer PDF for model parameters and a forward problem is to propagate uncertainties to calculate PDF for quantities of interest ^[1,4].

In computational fluid mechanics, it is now well known that assessment of accuracy and reliability of results of turbulent flow simulations is still a challenge and sometime, the reliability is typically case-dependent. Fortunately, UQ has already been broadly employed in quantitatively assessing uncertainty of accuracy and reliability to deeply understand physics of fluid and modelling, especially for turbulent flow simulations. UQ is capable to give hints on error dynamics and on reliability of simulated results ^[4].

By this talk, we briefly give an introduction of UQ in turbulent flow simulations and modelling applications. This talk highlights UQ in theory and applications, which covers the methodologies of RANS, LES, RANS-LES and DNS in computational fluid dynamics (illustrated in Fig. 1) ^[4-6]. The theoretical framework of UQ is presented based on the well-developed *Generalised*

Polynomial Chaos (gPC)^[1-2], which typically indicates a spectral decomposition of stochastic processes in terms of an orthogonal basis. In gPC, response of output quantities in parameter space is obtained by a truncated finite summation form of the orthogonal expansion. In practice, we choose the type of independent variable in polynomials according to the type of random distributions. Here, we illustrate the correspondence of the type of Wiener-Askey polynomial chaos and their underline continuous random variables in Table 1^[8]. Generally, there are two kinds of strategies to implement gPC^[1,2]: (a) intrusive; (2) non-intrusive. For the intrusive formulation, all variables associated with random effects are represented in truncated expansions, which are substituted into governed equation system. The spectral expansion coefficients are determined by the so-called *Galerkin* projection, which results in a series of governing equations from the original equation system. The non-intrusive formulation relies on a set of deterministic model resolutions which are corresponding to some specific values or realisations to construct the model output of interest parameterised by a finite set of independent random parameters. Compared with the intrusive formulation, the non-intrusive formulation is quite similar to data post-processing. The most attractive feature of non-intrusive formulations lies in the approximation of the model output of interest which needs a deterministic solver only.

Along with the theoretical framework of gPC, it will be explained that why UQ is now crucial to modelling and simulations of turbulent flows. As a further extension, some examples and recent attractive topics are illustrated in exploring transitional flows with uncertainty.

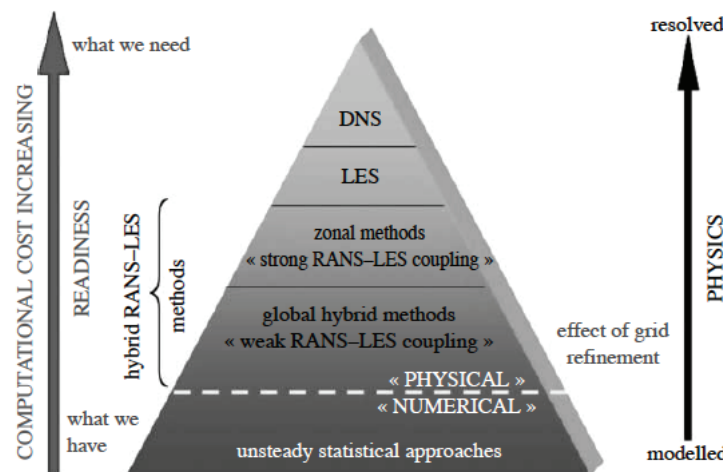


Figure 1 Classification of unsteady approaches according to levels of modelling and readiness^[7]

Table 1. Correspondence of the type of Wiener-Askey polynomial chaos to the type of random inputs^[8]

Random inputs	Wiener-Askey chaos	Support
Gaussian	Hermite-chaos	$(-\infty, \infty)$
Gamma	Laguerre-chaos	$[0, \infty)$
Beta	Jacobi-chaos	$[a, b]$
Uniform	Legendre-chaos	$[a, b]$

Reference

- 1 Le Maitre O P, Knio O M. Spectral methods for uncertainty quantification. Springer Dordrecht Heidelberg London New York, 2010.
- 2 Xu D B. Numerical methods for stochastic computations: A spectral method approach. Princeton University Press, 2010.
- 3 Tenorio L. An introduction to data analysis and uncertainty quantification for inverse problem. SIAM, 2017.
- 4 Oliver T, Moser R. Uncertainty qualification for RANS turbulence model predictions. APS, 62nd Annual meeting of the APS Division of Fluid Dynamics, Nov. 22-24, 2009.
- 5 Meyer J, Beurts B J, Sagaut P. Quality and Reliability of Large-Eddy Simulation. Springer, 2008.
- 6 Salvetti M V, Meldi M, Bruno L, Sagaut P. Reliability of large-eddy simulation: benchmarking and uncertainty quantification, in Direct and Large-Eddy Simulation X, edited by Grigoriadis D G E, Geurts B J, Kuerten H, Fröhlich J, Armenio V, Springer, Cham, p 15-23, 2018.
- 7 Sagaut P, Deck S, Terracol M. Multiscale and multiresolution approaches in turbulence. Imperial College Press, 2006.
- 8 Xiu D B, Karniadakis G E. Modeling uncertainty in flow simulations via generalised polynomial chaos. Journal of Computational Physics, 2003, 187: 137-167.

高坝水力学细观成因分析方法研究进展

许唯临，罗晶，卫望如，李瑶，张亚磊

四川大学 水力学与山区河流开发保护国家重点实验室

摘要：高坝水力学研究对于高坝工程泄洪安全以及其他类似问题具有十分重要的意义，随着高坝工程水力学指标的不断提高，更深入地揭示高速水流各种特殊水流现象的机理，从而为工程安全提供更加坚实的理论基础成为该领域亟待解决的问题。高坝工程中的空化空蚀、水流掺气等各种特殊水流现象几乎都是发生在细观尺度，而传统的高坝水力学研究主要采用宏观参数描述水流运动，难以准确反映高速水流的非连续性特征。近年来，作者不断探索高坝水力学细观成因分析方法，本研究重点对其中的空化泡近壁溃灭致蚀、掺气减蚀、高速水流自掺气和沙粒减蚀作用等进行了简要归纳。

关键词：水力学，高坝，细观

1 引言

我国的水能资源居世界首位，约占世界总量的 12%。由于国家经济发展对能源的迫切需求，我国的高坝工程发展迅速，特别是西南地区已成为世界上高坝大型水利水电工程最集中的区域。该地区不仅工程数量多，而且由于地理和气候的原因，许多工程拥有世界最高的技术指标，因此工程中的水力学问题十分突出。

高坝水力学的主要目标是保证高坝工程的泄洪安全。实际工程中因水力学问题而导致的不同程度的工程破坏大量存在，有些甚至对整个工程造成巨大威胁。高坝工程中主要的水力破坏方式是冲刷和空蚀。为了避免高坝下泄的巨大流量造成严重的冲刷破坏，必须在水流抵达下游固体边界之前大量消耗其动能，即所谓消能。但不幸的是，消能意味着强力干扰水流运动，因此消能效率越高往往意味着空蚀破坏的风险越大。防冲刷和防空蚀之间的这种相互矛盾的关系，使得保证高坝工程泄洪安全的难度大大增加。

传统的高坝水力学研究方法主要是对宏观变量的认识和描述，如流量、断面平均流速、压强等，其理论基础是由流体力学基本方程积分得到的伯努利方程以及动量方程和连续性方程，这种高坝水力学方法可以称之为宏观的总流方法。至 20 世纪后期，随着计算机技术的发展和数值计算水平的提高，对越来越多的高坝水力学现象实现了数值模拟，与宏观的总流方法相比，数值模拟直接立足于流体力学微分方程组，因此可以详细地给出各种变量

的时空分布，这种高坝水力学方法可以称之为流场方法。然而，高坝水力学中各种特有的复杂水流现象基本上都是发生在细观尺度（即空气泡、空化泡、水滴尺度），宏观尺度的研究难以准确阐释高坝工程中高速水流的各种特殊水力学现象的机理，因此高坝水力学研究必须深化到细观尺度，这里将此类方法称之为细观成因分析方法。

2 空化泡近壁溃灭致蚀的细观研究^[1-2]

我国对于高坝工程泄水建筑物是按照无空化的要求设计的，但是由于空化现象存在比较明显的缩尺效应，设计阶段通过模型试验获得的无空化体型方案经常会在原型工程中出现空化。因此，一方面需要深入研究空化的缩尺效应问题（不幸的是这一问题迄今仍未取得突破性进展）；另一方面需要进一步掌握一旦发生空化时是否会导致空蚀破坏。后者包括两个环节，一是空化泡是否会在壁面附近溃灭；二是如果空化泡会在避免附近溃灭则应如何避免空蚀破坏。对于第二个问题，即避免空化泡对壁面产生空蚀破坏，工程中普遍采用的行之有效的措施是掺气减蚀，但对于第一个问题始终缺乏研究。一个典型的实例是黄河小浪底水利工程的孔板式泄洪洞，设计阶段的大量模型试验研究给出了无空化体型方案，但是在原型工程的运行监测中仍然观测到空化的出现，加之所在洞段是有压洞而没有设置掺气减蚀设施，所以空化的出现尤其令人担心。然而，关闸后的现场观察表明，泄洪洞并未遭到空蚀破坏。小浪底泄洪洞的实践表明，在空化空蚀研究中，不仅要掌握空化的初生情况，还应掌握空化是否会导致空蚀破坏。如果能对空化致蚀条件有深入的认识，高坝工程泄水建筑物的设计就可以从无空化设计发展到无空蚀设计。

作者对矩形孔板后的空化泡溃灭位置进行了研究，在水洞中采用高速摄像和水听器相结合的方法，系统观测不同孔板尺寸和来流条件下的空化泡溃灭位置（图 1）。通过大量观测，获得了空化泡溃灭位置云图（图 2）。与流场的数值模拟结果进行对比，可以清楚地看到空化泡溃灭位置与孔板后漩涡结构的密切关系（图 3）。

进一步，分析不同的孔板水头损失（反映孔板体型尺寸特征）和来流速度（反映来流条件）下的空化泡近壁溃灭情况，可以发现空化泡是否会在近壁区溃灭与孔板水头损失有着密切而清晰的关系（图 4），在该试验条件下，当 $\Delta p/\rho gh < 20$ 时，即使出现空化，空化泡也没有在近壁区溃灭，从而不会对避免造成空蚀破坏。虽然实验室的结果因缩尺效应的原因而不能直接套用到原型工程，但这一结果无疑对于此类过流体型后的空化空蚀问题提供了更加深入的认识。事实上，若将小浪底泄洪洞的数据点绘到图 4 中（忽略轴对称二维流动与平面二维流动的差异），其相对水头损失远远小于 20，所以即使有缩尺效应的影响，仍可表明小浪底泄洪洞在防止空蚀破坏方面是安全的，换言之，小浪底泄洪洞所采用的孔板式消能工是可以有条件地在今后的类似工程中加以推广应用的。

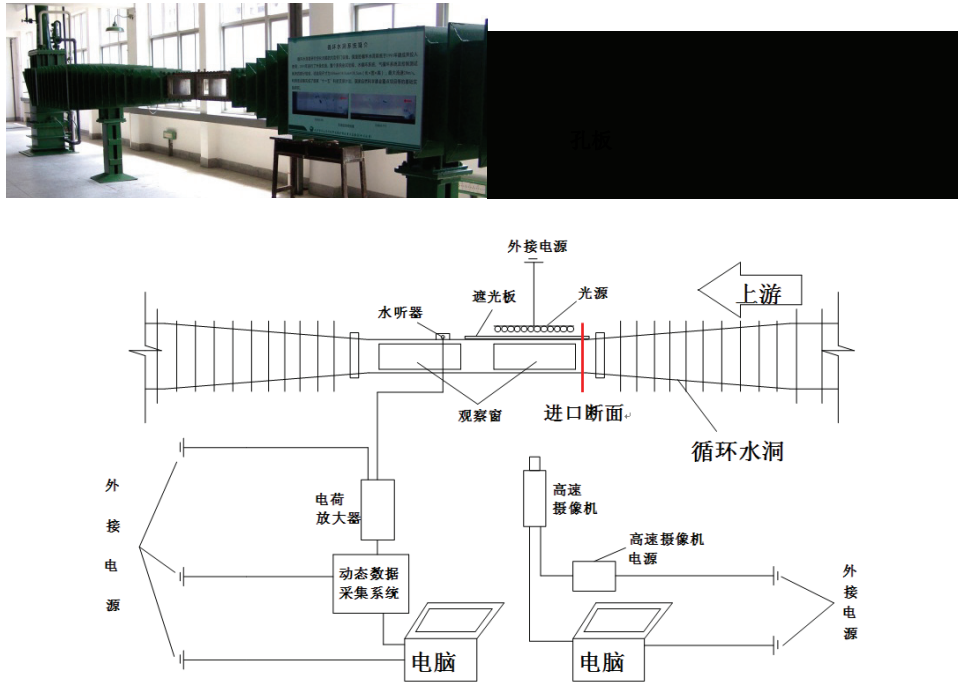


图 1 孔板后空化泡溃灭实验系统^[2]

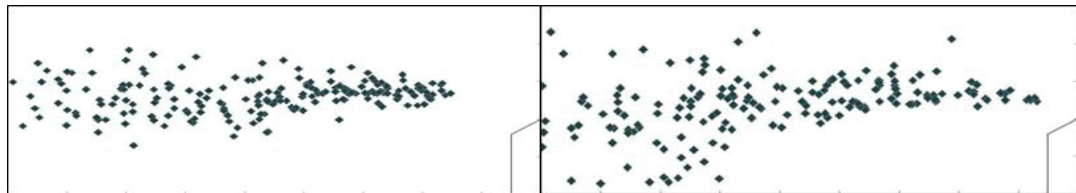
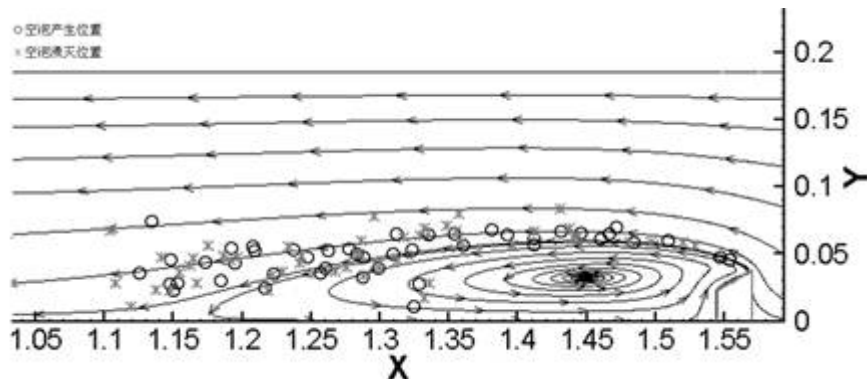
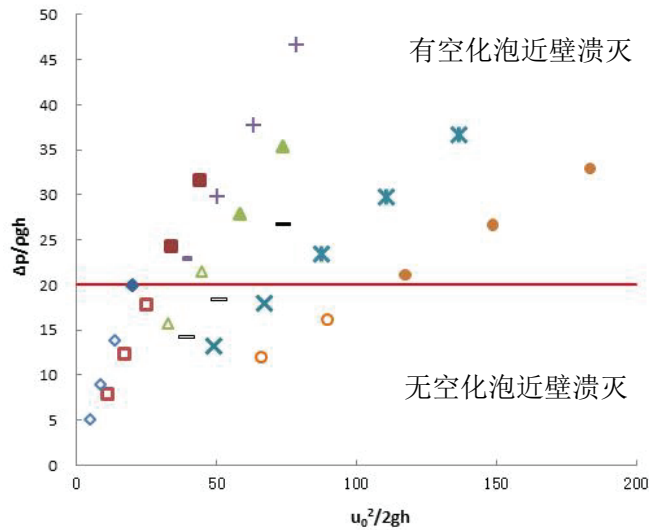


图 2 孔板后的空化泡溃灭位置^[2]

图 3 孔板后空化泡溃灭位置与水流流线的对照关系^[2]图 4 孔板后空化泡近壁溃灭条件分析^[2]

3 掺气减蚀机理的细观研究^[3-4]

当工程中由于水流条件和过流体型等原因而致使空蚀破坏难以避免时，最有效的手段便是设法向水体中掺入空气泡，即所谓掺气减蚀。然而，关于掺入空气泡后为何能够减免空蚀破坏，已有的解释众说纷纭，但都缺乏直接的证据。为此，作者研制了电火花空化实验装置（图 5），它与水洞和减压箱相比的最大优点是可以有效地控制空化泡的位置乃至尺寸。采用该装置和高速摄像系统，

可以直接捕捉空化泡、空气泡和壁面的相互作用过程。

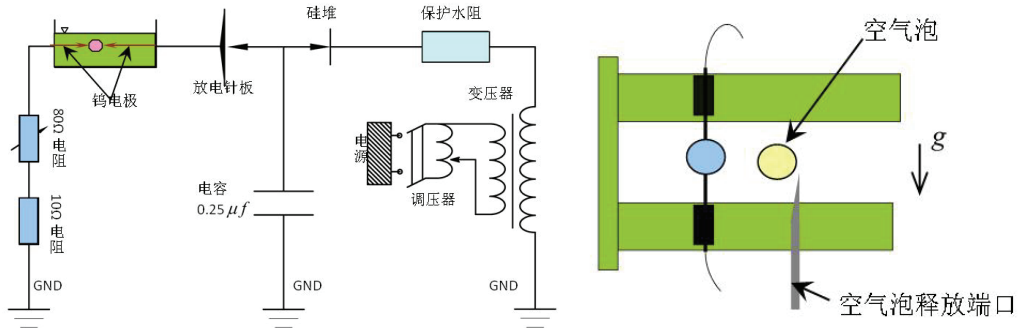


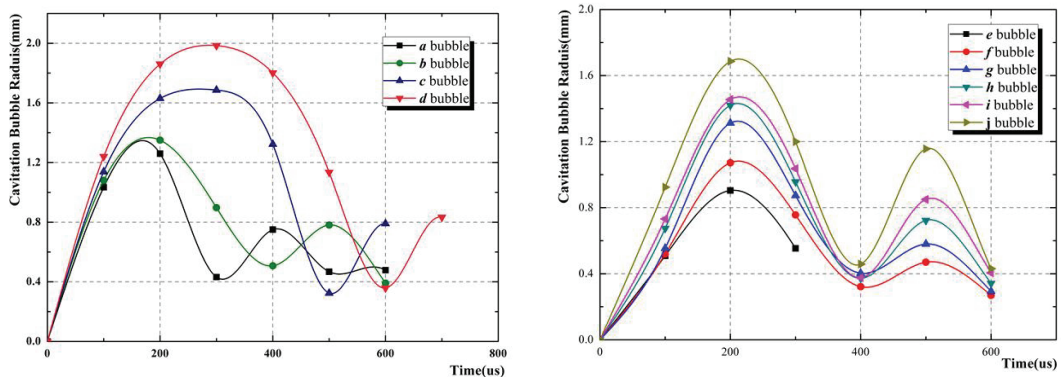
图 5 空化泡与空气泡相互作用实验系统^[4]

图 6 是采用上述实验装置拍摄的壁面附近空化泡与空气泡的相互作用情况。可以看到，当空气泡与空化泡相距较远时，空气泡可以阻滞空化泡的溃灭冲击波（图 6 左）；当二者距离相对较近时，空气泡可以改变空化泡的溃灭方向，使得原本朝向壁面溃灭的空化泡变成沿着壁面和空化泡的矢量合成方向溃灭（图 6 中）；当二者距离足够近时，空化泡与空气泡合并成含空气型空化泡（图 6 右），此时水听器测得的溃灭噪声强度大幅降低。这里将上述现象称为空气泡减免空蚀破坏的阻滞—变向—归并效应。传统上对于掺气减蚀效果的评价完全归结于掺气浓度，而从阻滞—变向—归并效应可知，在减免空蚀破坏的过程中，空气泡的个数比总体掺气浓度具有更加重要的作用。



图 6 空气泡对空化泡的阻滞—变向—归并作用

实验中还发现空气泡的存在对于空化泡的发展和溃灭周期有着明显的影响（图 7）。在没有空气泡存在的条件下，不同空化泡的发展和溃灭周期与空化泡的尺寸有着正相关的关系，空化泡尺寸越大，其发展和溃灭周期也越长（图 7 左）；但在附近有空气泡存在的条件下，不同大小空化泡的溃灭周期趋于一致（图 7 右）。

图 7 空气泡的存在使空化泡的发展和溃灭周期趋同^[4]

4 高速水流自掺气的细观研究^[5-6]

具有自由面的水流在速度达到一定程度时，将出现水滴脱离主流跃移到空气中以及空气被卷入水体成为气泡的现象，被称为高速水流自掺气。在高坝水力学中，掺气水流具有正反两方面的作用，一方面掺气可以减免空蚀破坏；另一方面掺气将不同程度地增加水深，从而会迫使溢洪道的边墙高度或泄洪洞的洞高相应增加，工程成本有所提高。因此，对于掺气水流的研究在高坝水力学中具有重要的意义，而掺气水流研究的基础是掺气成因。

已有的关于掺气水流成因的研究结果主要有波浪破碎理论、边界层发展理论、紊动强度理论和水滴运动理论。随着试验技术的发展，现在可以更加详细地观测掺气水流的形成过程，从而更加深入地了解掺气水流的成因。作者在前人研究的基础上，对掺气水流的形成过程进行了大量的细观观测，一方面进一步证实了高速自由面流动条件下，水滴克服表面张力作用跃出水面的过程；另一方面也揭示出自由面变形裹挟空气形成气泡的过程。前者与前人的研究结论一致，而后者则有所不同（图 8）。

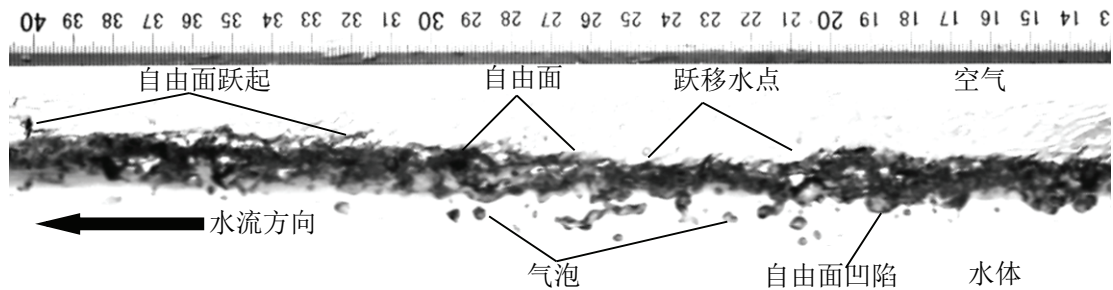


图 8 高速水流自由面附近的水滴跃移和气泡卷入

实验表明，高速水流在紊动作用和水气边界剪切作用下，其自由面剧烈变形，当变形达到一定条件时，自由面无法恢复，凹陷处的底部被周围水体封闭成为独立的空气泡，空气泡在紊动作用下可以向水流核心区扩散，在一定条件下甚至可抵达水流底部边界，从而使整个水体成为水气二相流（图9）。这一结论更符合掺气水流的实际情况，特别是空中自由射流和高坝工程中常用的底部强迫掺气设施的下自由面掺气情况。基于上述机理，可以建立一套比较完整的高速自掺气水流计算方法^[5]。

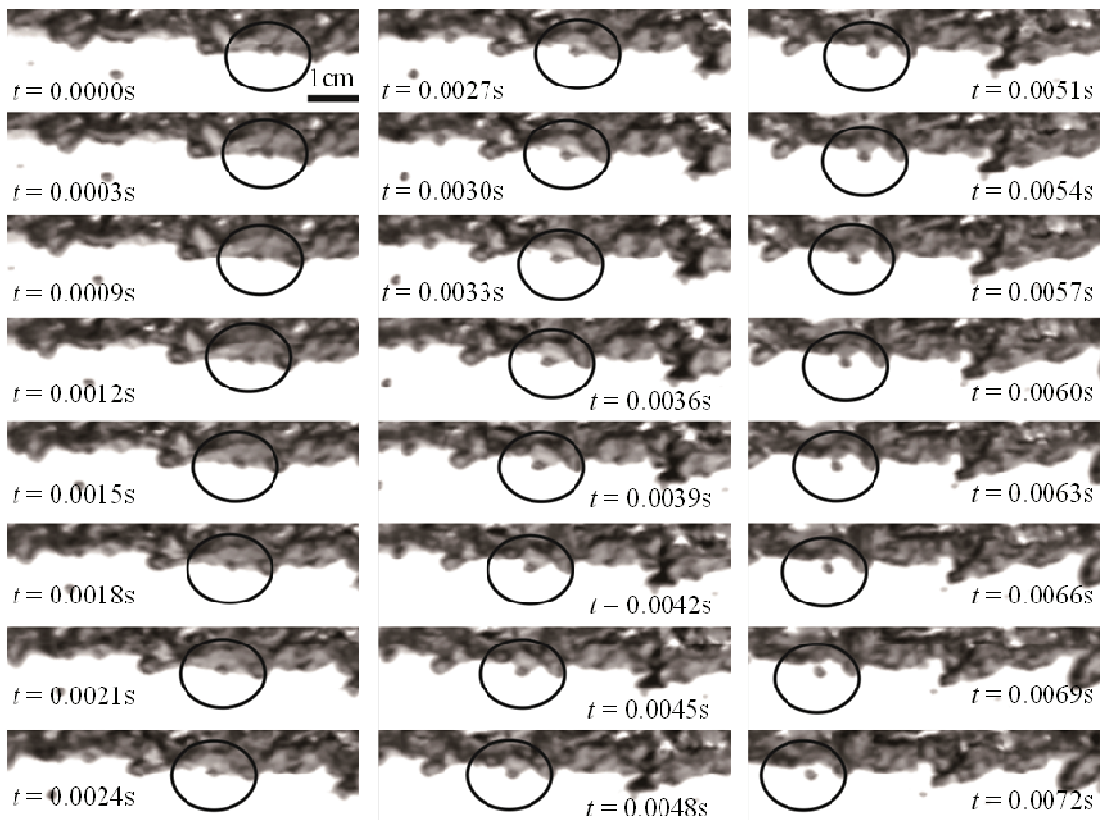


图9 自掺气水流的气泡卷入过程

5 沙粒减蚀作用的细观研究^[7-8]

高坝工程下泄的高速水流中常常或多或少地含有泥沙，对于沙粒的作用，以往主要关心的是其增加了磨蚀，事实上，沙粒在增加水流磨蚀的同时，还具有减免空蚀的作用，这与壁面吸引空化泡的作用是相似的。图10显示了沙粒附近电火花空化泡的溃灭过程，可以看到，即使沙粒尺寸小于空化泡尺寸，它仍然可以吸引空化泡朝向其溃灭。这意味着在一

定条件下，沙粒的存在有助于避免空化泡打击壁面，从而起到减免空蚀破坏的作用。

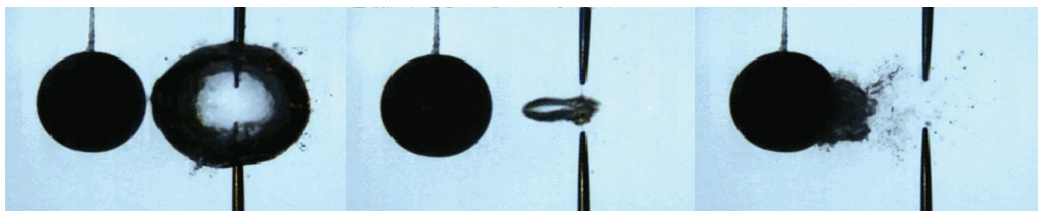


图 10 空化泡朝向沙粒溃灭^[8]

进一步的分析表明，沙粒吸引空化泡的作用与沙粒和空化泡的相对尺寸以及相对距离有关。从图 11 中可以看到，随着相对尺寸和相对距离的不同，沙粒对于空化泡溃灭的影响大致可以划分为朝向区、过渡区和无影响区 3 个区域，其中尤其令人感兴趣的是，较小的沙粒相对尺寸反而具有较大的相对影响距离，这意味着较小的沙粒在降低磨蚀作用的同时，仍可较好地发挥减免空蚀的作用。

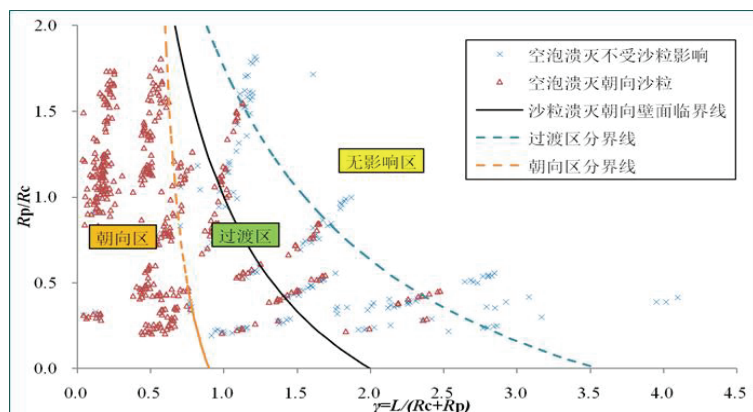


图 11 沙粒对空化泡溃灭影响的分区^[8]

以上简要回顾了空化泡近壁溃灭致蚀、掺气减蚀机理、高速水流自掺气和沙粒减蚀作用的细观尺度研究进展，除此之外，近年来作者还对高速射流散裂、弹性壁面附近空化泡溃灭规律等进行了细观研究，在此不再一一赘述。

6 结语

上述结果中许多已经开始在工程中发挥出实际作用，譬如：基于凸体后空化泡溃灭位

置的细观规律，研发了有压泄洪洞渐缩突扩式消能技术；基于掺气减蚀的细观机制，研发了微掺气减蚀技术；基于高速水流自掺气的细观成因，建立了新的预测方法等等。但是，随着细观研究的不断深入，发现的新问题超过已获得的新结果，表明在细观探索方面还有很长的路要走。

参考文献

- 1 李瑶. 消能孔板后的空泡溃灭位置分布规律研究. 四川大学, 2013.
- 2 LI Yao, XU Wei-lin, ZHANG Ya-lei, et al. Cavitation bubbles collapsing characters behind a convex body. Journal of Hydrodynamics, 2013, 25(6):886-894.
- 3 罗晶. 空化泡与空气泡相互作用的规律研究. 四川大学, 2013.
- 4 LUO Jing, XU Wei-lin, NIU Zhi-pan, et al. Experimental Study on the interaction between the Spark-induced cavitation bubble and the air bubble. Journal of Hydrodynamics, 2013, 25(6):895-902.
- 5 卫望如, 明渠自掺气水流卷吸掺气机理及计算方法研究. 四川大学, 2018.
- 6 WEI Wang-ru, DENG Jun, ZHANG Fa-xing. Development of self-aeration process for supercritical chute flows. International Journal of Multiphase Flow, 2016, 79:172-180.
- 7 张亚磊, 两相流中空化泡的溃灭特性. 四川大学, 2016.
- 8 XU Wei-lin, ZHANG Ya-lei, LUO Jing, et al. The impact of particles on the collapse characteristics of cavitation bubbles. Ocean Engineering, 2016, 131:15–24.

Progress in meso-scale causal analytic method of high dam hydraulics

XU Wei-lin, LUO Jing, WEI Wang-ru, LI Yao, ZHANG Ya-lei

State Key Lab. of Hydraulics and Mountain River Engineering , Sichuan University

Abstract: High dam hydraulics plays a major role in solving the problems of flood discharge safety in high dam engineering. Almost all of the special flow phenomena in high dam engineering (e.g. cavitation, aeration etc.) occur in meso-scale between macro-scale (engineering scale) and micro-scale (molecule scale). However, in the traditional method of high dam hydraulics, flows are described by macro-scale

variables such as flow rate, velocity, pressure and water depth, so that discontinuous flow phenomena as above-mentioned can not be analyzed directly. In the recent years, authors have been exploring the meso-scale research on high dam hydraulics, some results about the collapse position of cavitation bubbles, interaction between a cavitation bubble and an air bubble, self-aeration at free surface etc. are summarized in this review.

Key words: hydraulics, high dam, meso-scale

PIV and its application in hydrodynamics of cylindrical structures

WANG Xi-kun^{1,2}

¹ Maritime Research Centre, Nanyang Technological University, 50 Nanyang Avenue, 639798,
Singapore

² National Research Center of Pumps, Jiangsu University, Zhenjiang Jiangsu 212013, China

Email: cwkwang@ntu.edu.sg

Abstract: During the past three decades, Particle image velocimetry (PIV) has evolved rapidly to be the dominant method in experimental fluid mechanics and has contributed to many advances in our understanding of turbulent and complex flows. In this paper, we provide a brief review the achievements of PIV and its latest developments: e.g., time-resolved PIV; statistical PIV; tomographic PIV. In the actual implementation of PIV, however, there are a lot of pitfalls that may lead to inaccurate or even erroneous results. Therefore, we compile our knowledge and experience about PIV accumulated over past years, and provide some practical guidelines for its implementation in practice to obtain accurate results. This paper focuses on the application of PIV in investigating the hydrodynamics of cylindrical structures, since it is fundamental in many engineering applications such as heat exchange tubes, transmission lines, piers, pipelines, risers. A wide range of flow configurations are considered, including: (a) a cylinder (circular/square) placed in proximity to a wall boundary; (b) two tandem cylinders (circular/square) placed in proximity to a wall boundary; (c) multiple cylinder arrays; (d) cylinders with rough surface for drag reduction; (e) cylinder undergoing vortex-induced vibration (VIV); and so on.

Key words: Particle image velocimetry (PIV); Hydrodynamics of cylindrical structures; Vortex-induced vibration (VIV)

1 Introduction

The dream of experimental fluid dynamicists is to be able to measure complex, 3-dimensional (3D) turbulent flow fields globally with very high spatial and temporal resolution.

Although we are still far from fully realizing this dream, significant progress has been made towards this goal. Traditionally, “point-wise” measurement techniques, such as Hot Wire Anemometry (HWA) and Laser-Doppler Anemometry (LDA), are used to measure the instantaneous velocities at a particular point through time. Early emphasis in turbulence research and its theoretical advancement necessitate a statistical description of turbulent flow fields based on the measured signal. However, it is difficult to obtain the accurate and detailed information of the global flow field that is transitional and spatially evolving. Therefore, there is much interest in pursuing the goal of nonintrusive, “global-wise” (whole-field) velocity measurements. Concurrent with rapid developments in modern imaging, laser, and data acquisition and processing technology, a relatively new measurement technique, Particle Image Velocimetry (PIV), has become the standard global-wise tool in experimental fluid mechanics since its first invention in 1980’s [1]. The principal characteristic that has made it so useful is its ability to measure the instantaneous velocity field simultaneously at many points, typically of the order of 10^3 – 10^5 , with spatial resolution sufficient to permit the computation of the instantaneous vorticity and rate of strain. To date, PIV is the only experimental method that provides such information in turbulent flows [2]. PIV has been reviewed in the literature several times [2-6] and is also the subject of two books [7-8]. The reader is referred to these materials for a detailed description of state-of-the-art of the technology in a broad sense, i.e., including approaches such as particle tracking velocimetry (PTV), microscopic PIV, holographic PIV and tomographic PIV.

Successful usage of PIV, however, requires a good understanding of the operating principles; it cannot realistically be treated as a ‘black box’ or ‘plug and play’ system. Therefore, we compile our knowledge and experience about PIV accumulated over the past 15 years, and provide some practical guidelines for its implementation in practice. Section 2 briefly introduces the basic working principles of PIV, and some critical considerations in PIV measurements. Section 3 reviews several major developments and milestones in PIV. A list of applications of PIV in the investigation of hydrodynamics around cylindrical structures is given in Section 4. Section 5 summarizes the contemporary PIV technique in terms of its pros/cons and proposes some recommendations for its utilization.

2 Basic PIV system(2D-2C)

PIV is a technique that allows for instantaneous measurement of the flow velocities at many points in a plane. A typical setup is shown in Figure 1, which can measure 2 velocity components in a 2-dimensional (2D) plane using a single camera (facing normal to the plane), and hence is referred as 2D-2C PIV (or simply 2D PIV, or planar PIV) configuration. Other configurations,

such as 2D-3C (2-dimension/3-component) and 3D-3C (3-dimension/3-component, which is truly 3D) will be introduced in Section 3. 2D-2C configuration is the simplest and therefore the most widely deployed of PIV.

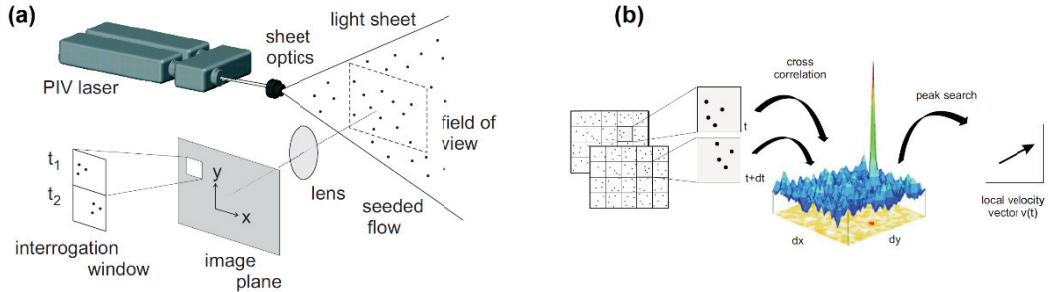


Fig. 1 Working principle of PIV (Adapted from LaVision user manual^[9])

2.1 Working principle of PIV

The working principle for PIV is relatively simple (c.f. Figure 1): the flow is seeded with light scattering particles, a light sheet (generally laser) illuminates the particles in the measurement plane and a camera lens images the target area onto the CCD array of a digital camera. The CCD is able to capture each light pulse in separate image frames. Once a sequence of two light pulses (with a time delay Δt) is recorded, the images are divided into small subsections called interrogation areas (IA, typically 32×32 pixels in size). The IAs from each image frame are cross-correlated with each other, pixel by pixel. The correlation produces a signal peak, identifying the common particle displacement, ΔX . An accurate measure of the displacement, and hence the velocity ($\Delta X / \Delta t$), is achieved with sub-pixel interpolation. By repeating the cross-correlation for all IAs over the whole target area, the 2D velocity vector map in this plane is obtained.

Presently, the single-camera, planar light sheet, cross-correlation PIV with a double-pulsed Nd:YAG laser and a 2K×2K-pixel cross-correlation CCD camera is the standard system sold by commercial companies. In turbulence research, just using simple 2D PIV has been enormously rewarding in revealing fundamental aspects of the turbulence structure. More sophisticated forms of PIV are emerging and will definitely impact efforts to understand turbulence, but one should not rush into complexity before mining the wealth of information that can be achieved using 2D PIV. However, there are a lot of issues to take into account for a successful implementation, which are highlighted below.

2.2 Tracer particles

Tracer particles play a key role in PIV measurements, because PIV actually measures the velocity of tracer particles instead of real fluid velocities. The first consideration is their size. It

should be small enough to achieve good tracking behavior of the flow but large enough to scatter sufficient light signal for image recording devices. Table 1 lists typical tracer particles used for air and liquid flows. In general, acceptable tracking ability is more crucial for the study of turbulent in a small region, whereas the scattering demand should be more concerned for large-scale measurements. For liquid flows, particle diameter of 10-20 μm is a good compromise. For gas flows, in comparison, due to the great difference between the index of refraction of gas and particles, small particles in gas scatter enough light to be detected; therefore, particle diameter of 1-5 μm is generally used. In summary, the size of the tracer particles should be optimized to make a balance between the tracking behavior and the scattering characteristics depending on the application.

Table 1 Typical tracer particles for gas and liquid flows

	Material	Mean diameter in μm
For Gas flow	Polystyrene	0.5-10
	smoke	< 1
	magnesium	2-5
	different oils	0.5-10
For liquid flow	Polystyrene	10-90
	aluminum	2-7
	glass spheres	10-100

The second consideration is the density of tracer particles. It is desirable for the particles to be neutrally buoyant, which is, however, difficult to achieve in practice, particularly for gas flow. Therefore, the influence of gravitational forces cannot be neglected. One need to employ the Stokes' drag law to estimate this effect called velocity lag:

$$u_g = d_p^2 \frac{\rho_p - \rho_f}{18\mu} g \quad (1)$$

where g is the gravitational acceleration, ρ_f and μ are the density and dynamic viscosity of the fluid, ρ_p and d_p are the density and diameter of the particles. Eq. (1) indicates that the diameter of non-neutrally buoyant particles should be small enough to reduce the velocity lag. For PIV application, the particle's response to the flow can be quantified by the relaxation time of the particles:

$$\tau_p = d_p^2 \frac{\rho_p}{18\mu} \quad (2)$$

Nevertheless, the Stokes' drag law may underestimate the actual velocity lag in flows with high turbulence level. The maximum allowable particle size decreasing with increasing flow velocity, turbulence level and velocity gradients.

The third issue is the seeding concentration. Particles should be seeded into the flow with sufficient, steady and spatial uniform concentration. Generally, a higher seeding concentration is preferred for better measurement spatial resolution. However, excessive high seeding concentration may lead to poor spatial resolution due to bad scattering performance. The ideal concentration is 10–20 particles per an IA^[7]. A uniform seeding size is also desirable in order to avoid excessive intensity from larger particles and background noise and incoherent signals from smaller particles. It is recommended to use a particle counter to analyze the particle size distribution during the measuring process. The seeding method can be divided into global seeding and local seeding. Global seeding is feasible in small-scale model and re-recirculating flowsystem to achieve the whole velocity measurement. However, global uniform seeding in large-scale model may always be restricted to the generation capacity. Then one might consider local seeding to the region of interest. In this case, the position of seeding probes should be carefully positioned in order not to disturb the flow.

2.3 Illumination system

The most widely used illumination system for PIV is a double-pulsed Nd:YAG laser system with an articulated delivery arm to generate a green light sheet of 532 nm wavelength. The pulse durations of Nd:YAG laser are short enough, about 5~10 ns, to effectively freeze the images of particles moving at all but the hypersonic velocities. Pulse energies range from 5 to 800 mJ, depending on the size of the illuminated region. The light sheet optics locate at the end of the arm can be oriented at any angle to generate a light sheet and illuminate the tracer particles in the measured region of interest. The main component of light sheet optics is one or more cylindrical lens to focus the light sheet to desired thickness and field angle. To guarantee the measured flow field can keep in a plane, and the thickness of light sheet in the measurement area is typically about 1–2 mm or less. An important parameter to set is the inter-pulse time delay, Δt . The time delay should not only be long enough to determine the displacement of particles between the two pulses, but also need to be short enough to avoid particles moving too far away. It has been established that for each image pair, the separation (in pixels) should be larger than the accuracy of peak detection (~ 0.1 pixel), but smaller than a quarter of the size of each IA (or the $\frac{1}{4}$ law). Therefore, the pulse delay, which depends on the desired IA size (Δ_{IA} , in pixels) and on the maximum flow velocity, consequently will be in the range of:

$$\frac{\Delta t \cdot U_{\max}}{\Delta_{IA}} \leq 1/4 \quad (3)$$

2.4 Image recording device

The most common image recording devices for PIV are coupled charged devices (CCD) camera, for their superior spatial resolution, convenient data transmission and image processing, short exposure time, high light sensitivity and low background noise. Today, commercially

available CCD cameras typically have sensor resolutions ranged from 1M (1024×1024 pixels) to 29M (6567×4384 pixels), and frame rate from 35 Hz to 2 Hz. The higher the resolution, the lower the frame rate. Thus, one should make a trade-off between the spatial resolution and the temporal resolution depending on specific applications. For example, a high resolution camera is necessary for large-scale models; conversely, a high frequency camera is more suitable for studying small-scale turbulent characteristics. In addition, the dynamic range of CCD sensors should also be considered to evaluate the signal quality per pixel. Normally, a dynamic of 8 or 10 bits is sufficient for most PIV applications. However, with advanced cooling technique, 14- or 16-bit camera is also available. For time-resolved PIV, a high-speed complementary metal oxide semiconductor (CMOS) camera is a better choice than a CCD camera. High-speed recording based on recently developed CMOS sensors even allows for acquisition at the order of kHz, but in trade of sensor resolution. A detailed comparison between CCD and CMOS cameras is reported by in [10].

2.5 Image evaluation methods

Particle images from the first laser pulse are stored in the first camera frame, and images from the second pulse go into a separate, second frame. This two-frame recording determines unambiguously the direction of the displacement between any pair of particle images, and it allows the analysis of overlapping images, thereby eliminating the need to employ image shifting (Adrian 1986). The displacement of the particle images in each IA is measured by cross-correlating the images of the first and second frames to find the mean displacement that gives the maximum correlation. The velocity estimate is assigned to the center of the interrogation region if the displacement is small compared to the IA size, or to the midpoint of ΔX if the displacement is large, corresponding to a central difference estimate [8]. The analysis is performed on a set of interrogation domains that covers the measurement area, typically with windows overlapping 50% or 75%. The smaller IA size and higher overlap ratio can achieve higher spatial resolution, but require higher quality image recordings and consume longer computing time. This is one limitation of PIV that in a region with intensive velocity gradients, correlation algorithm averages particle motions in the interrogation window resulting in an underestimation of velocity gradient. The adaptive correlation method can achieve higher accuracy supplemented with high sub-pixel accuracy and adaptive deforming window algorithm. Currently, adaptive correlation is available in most of the commercial PIV software packages.

2.6 Performance of 2D PIV

At present, the 2D PIV technique is well established and the processing algorithms are near optimum. Once applied properly, a typical planar PIV system is capable of recording images that yield typically 10^4 measurements of the velocity (per image frame pair) with an accuracy of approximately 1%–2% of the full-scale displacement range. Frame rates have increased

dramatically with the introduction of new cameras and high-repetition-rate lasers, and this development offers a straightforward path for the expansion of PIV capability to time-resolved PIV (TR-PIV). Coupling PIV with simultaneous planar laser-induced fluorescence (PLIF) has also enjoyed great success [11]. Making combined measurements of fluid velocity and the velocity of a second phase such as particulate, droplet or vapor phase is a viable and valuable extension of PIV into multi-phase flow. The simultaneous measurements of liquid velocity and bubble phase by [Lindken and Merzkirch](#) [12] is an excellent example.

3 Advanced PIV techniques

The “classical” 2D PIV is only capable of measuring two components of velocity vectors in the plane of the illuminating laser sheet. To study more complex flow phenomenon, several advanced PIV techniques have been developed in recent years, such as stereoscopic PIV, time-resolved PIV, statistical PIV, 3D volumetric PIV, among others.

3.1 Stereoscopic PIV (2D-3C)

The inherent limitation of the 2D-2C method is that only two components of the velocity vector are resolved. Therefore, it is perfectly suitable for nominally 2D flow; for 3D turbulent flow, it should be used and interpreted with care. The unresolved out-of-plane velocity component also leads to a ‘perspective error’ [7] in the resolved components, particularly for wide-angle camera lenses. This error can be addressed by 2D-3C stereoscopic PIV, which makes it possible to reconstruct all three velocity components in a planar cross section. This kind of system requires at least 2 cameras which are oriented such that they view the same flow region from different angles. If the camera viewing angle is large, the camera lens may be tilted with respect to the camera to re-align the plane of focus of the camera with the light sheet, i.e., the so-called “Scheimpflug” condition [13]. Furthermore, dual-plane PIV provides access to the full deformation tensor in a planar cross section of the flow [14].

Strictly speaking, stereo 2D-3C PIV does not belong to 3D PIV, since only the three velocity components on a particular plane are measured. Although Stereo 2D-3C PIV is relatively common now days, the out-of-plane component is inherently less accurate than the in-plane components. Also, the thin light sheet as the illumination method brings about a challenge for measuring a strong 3D flow field in sizeable flow domain. In this case, some particles recorded by the cameras in the first frame may move out of the relatively thin sheet and cannot be captured in the next frame, leading to out-of-plane loss-of-pairs. These factors limit the application of 2D-3C PIV in strongly 3D flows.

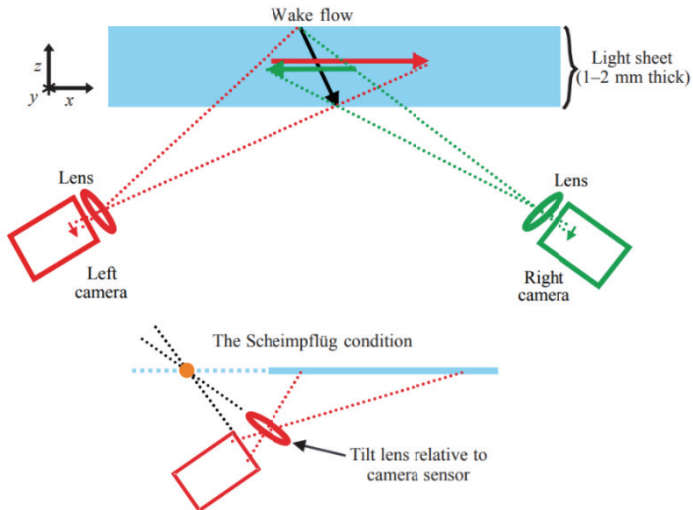


Fig. 2 Working principle of 2D-3C stereoscopic PIV (Adapted from Nauen & Lauder^[15])

3.2 Time-resolved PIV (TR-PIV)

The temporal evolution of turbulent velocity fields can be measured by dynamic, high-speed, or time-resolved PIV (TR-PIV) systems. TR-PIV is conceptually straightforward, and its technical achievements are determined principally by the performance of available light sources and cameras. In particular, double pulsed Nd:YLF lasers are capable of generating 10–20 mJ per pulse and up to 10,000 pulses per second. These are typically combined with CMOS cameras that can record $1\text{K} \times 1\text{K}$ -pixel images at framing rates up to 5,000 frames per second. (Higher frame rates are achieved for reduced-image formats.) Hori & Sakakibara^[16] used a stereoscopic TR-PIV system combined with a scanning light sheet to record a volumetric domain of a low-Reynolds number free jet. In addition, TR-PIV time sequences of stereoscopic PIV data and Taylor's frozen-field hypothesis can be used to reconstruct the quasi-instantaneous 3D vortical structures in the flow, such as for localized turbulence (or puffs) in transitional pipe flow^[17] or vortex packets in a turbulent boundarylayer^[18]. To date, the sampling rate (frequency) of TR-PIV has reached 50 kHz. More recently, Beresh et al.^[19] used an extraordinarily high-speed TR-PIV at 400 kHz for sequences exceeding 4000 frames but for an array of only 128×120 pixels, giving the moniker of 'postage-stamp PIV'. The technique has been tested far downstream of a supersonic jet exhausting into a transonic crossflow, and two-component measurements appear valid until 120 kHz.

3.3 Statistical PIV

There is a growing body of experimental studies in which PIV is used not to measure the instantaneous fields, but instead to measure the flow statistics such as mean velocity or various

components of the Reynolds stress tensor. This approach is particularly well suited to inhomogeneous turbulent flow in complicated geometries. In this method, the local spatial correlation functions of the images in interrogation spots are averaged over the ensemble and then the mean statistics are extracted from the mean correlation function at each interrogation spot. The correlation averaging technique was developed for multiphase flow^[20] and microscopic PIV^[21]. This approach is executed with very high spatial resolution by employing the single-pixel correlation method^[8], and it has been utilized with impressive results^[22-23].

3.4 Three-dimensional (volumetric) PIV (3D PIV)

Attempts of volumetric PIV measurement were long-lasting and started since mid-1990s, such as defocusing PIV, scanning light sheet (SLS) PIV and holographic PIV (see reviews in [6]). Unfortunately, those PIV techniques are not widely used due to some limitations (e.g., poor spatial resolution in defocusing PIV or SLS PIV, small measurement volume in holographic PIV). Elsinga et al.^[24] proposed a new concept of ‘tomographic PIV’, which provides a better spatial resolution and turns to be the most promising technique for volumetric measurements. Here, the current status and capabilities of tomographic PIV are briefly reviewed. Details about can be found in the reviews by Scarano^[5] and Discetti & Coletti^[6].

Tomographic PIV belongs to a multi-view PIV method (see Fig. 3). The key idea of tomographic PIV is reconstructing 3D particles using tomography technique, which is a mature method of medical diagnosis known as computed tomography (CT). In this approach, the tracer particles are illuminated within a volume (a fat-sheet with a thickness of about one-quarter the width or length of the field of view), and the light scattered by these particles is recorded from several viewing directions simultaneously, typically using four to six cameras. To keep all particles within the volume in focus, one generally requires the use of Scheimpflug adapters and a small aperture, or large f #, for the camera lenses. From the recordings, the particle distribution is reconstructed as a 3D light-intensity distribution discretized onto voxel elements, which are the volumetric equivalent of pixels. A constraining factor in all tomographic PIV experiments is the measurement error introduced by reconstruction. The error has multiple sources: imaging artifacts (e.g., out-of-focus blur^[25]), calibration inaccuracies^[26], background reflections and camera noise; however, the predominant source is due to ghost particles^[24], which is a key issue in volumetric PIV. The MART (multiplicative algebraic reconstruction technique) algorithm developed by Elsinga et al.^[24] can still be considered the standard; however, in recent years a portfolio of feature-oriented reconstruction techniques has flourished. The full three component velocity field is then computed via 3D digital cross-correlation of the reconstructed volumes at a more confidence level, and this technique will become mature in the near future.

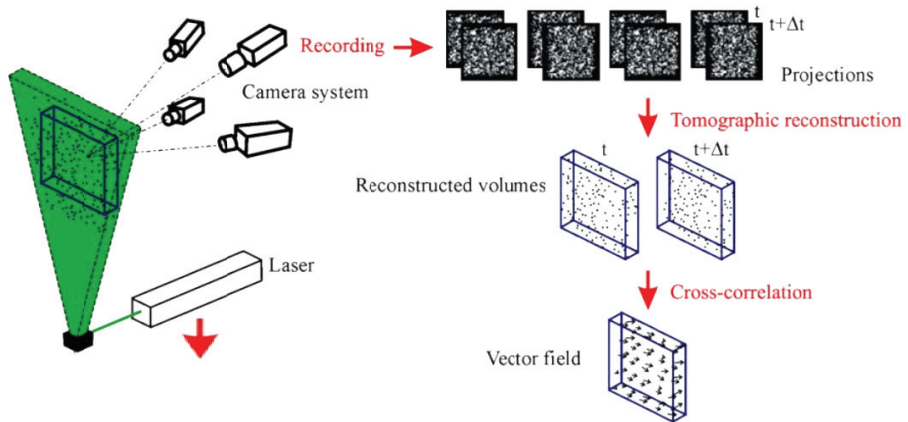


Fig. 3 Tomographic PIV (reproduced from Elsinga et al. [24])

However, Tomographic PIV still has some limitation factors to hinder its wide applications, including:

- High lighting power is required for illumination of a volume;
- The size of recorded images needs to be much larger than for regular planar or stereo PIV;
- The hardware used are of high cost and presents some safety concerns;
- Large computational power is required to analyze the recorded images as compared with conventional planar PIV;
- Complicated and sensitive 3D calibration procedure.

3.3 4D-PIV (3D + time-resolved)

Time-resolved measurement regime for PIV enables time-domain analysis (e.g. time correlation) and description of the spectral content of the fluctuating velocity field with fine enough time-resolution (satisfying the Nyquist criterion). Time-resolved 3D PIV, or 4D PIV, is characterized by a high degree of spatial and temporal coherence between subsequent 3D volumetric measurements. This is realized by recent developments of Tomographic PIV for application in moderate Reynolds number, by using high-speed camera and laser systems to acquire image sequences typically composed by hundreds or thousands of recordings. For instance, LaVision GmbH developed a 4D PIV technique using four high-speed video cameras, capable of 1200 frames/sec at full resolution of $2K \times 2K$ pixels. As a result, the spatial and temporal development of a flow is vividly captured. The breadth of information contained in these sequences has led to its application to investigate unsteady flow phenomena in their 3D structure (such as all components of vorticity and velocity gradient tensor), but also to follow their dynamical evolution and extract quantities such as the instantaneous pressure field. Among

the most prominent applications of time-resolved tomographic PIV are the unsteady pressure evaluation [27-28], aero-acoustic estimation [29]. 4DPIV offers the possibility of investigating fully 3D complex turbulent flow fields globally with very high spatial and temporal resolution.

4 Applications of PIV in hydrodynamics of cylindrical structures

This section illustrates some applications of PIV in the field of hydrodynamics of cylindrical structures in a water channel at Maritime Research Centre, Nanyang Technological University, Singapore. Velocity measurements were performed using a LaVision PIV system. The flow field was illuminated with a double cavity Nd:YAG laser light sheet (Litron model, wavelength ~ 532 nm, repetition rate ~ 15 Hz, power ~ 135 mJ per pulse, duration ~ 5 ns). Sphericel[®] 110P8 hollow glass spheres (neutrally buoyant with a mean diameter of $13\text{ }\mu\text{m}$) were seeded in the flow as tracer particles. The particle images were recorded using a 14-bit CCD camera, with a resolution of 1600×1200 pixels and a frame rate of 15 Hz. Particle displacement was calculated using the fast-Fourier-transform (FFT) based cross-correlation algorithm with the standard Gaussian sub-pixel fit structured as an iterative multi-grid method. The processing procedure included two passes, starting with a grid size of 64×64 pixels, stepping down to 32×32 pixels overlapping by 50%, which resulted in a set of 7500 (100×75) vectors for a typical field.

The 1st flow configuration is the near-wall cylinder to investigate the effects of wall proximity on the wake structure [30-31]. Fig. 4 shows the 2D PIV measurement results in the near wake of a circular cylinder located close to a flat wall. The Reynolds number based on the cylinder diameter (D) is 1.2×10^4 for various gap heights (S) between the cylinder and the wall. Both the ensemble-averaged (including the mean velocity vectors and Reynolds stress) and the instantaneous flow fields are strongly dependent on S/D . Results reveal that for $S/D \geq 0.3$, the flow is characterized by the periodic, Kármán-like vortex shedding from the upper and lower sides of the cylinder. For small and intermediate gap ratios ($S/D \leq 0.6$), the wake flow develops a distinct asymmetry about the cylinder centerline; however, some flow quantities, such as the Strouhal number and the convection velocity of the shed vortex, keep roughly constant and virtually independent of S/D .

The 2nd configuration considered is flow around two identical cylinders (square in [32] and circular in [33]) placed in tandem arrangement and near a plane wall. The inter-cylinder spacing ratio was varied from $S^* = 0.5$ to 6, and the cylinder-to-wall gap ratio from $G^* = 0.25$ to 2, in order to systematically investigate the effects of wall proximity and the mutual interference between the two cylinders in the normalized gap-spacing (S^*-G^*) plane. Fig. 5 presents the

instantaneous normalized vorticity fields obtained by 2D PIV.

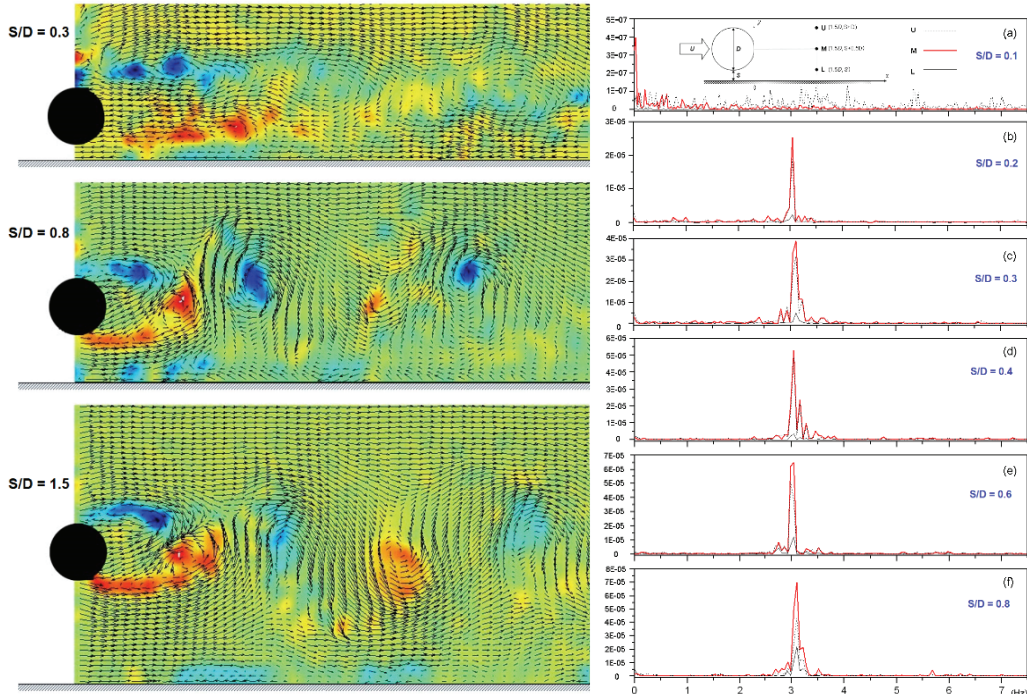


Fig. 4 2DPIV results on a near wall cylinder (reproduced from Wang and Tan^[30]). Left: Instantaneous velocity vector field superimposed with flood contours of spanwise vorticity; Right: power spectra of transverse velocity in the wake. $Re = 12,000$

The 3rd configuration is an array of four cylinders arranged in a square configuration [34]. The Reynolds number was fixed at $Re = 8000$, the pitch-to-diameter ratio between adjacent cylinders was varied from $P/D = 2$ to 5 and the incidence angle was changed from $\alpha = 0^\circ$ (in-line square configuration) to 45° (diamond configuration) at an interval of 7.5° . The flow interference among the cylinders is complicated(see Fig. 6), which could be non-synchronous, quasi-periodic or synchronized with a definite phase relationship with other cylinders depending on the combined value of α and P/D . Together with PIV measurements of the flow field, the fluid dynamic forces (lift and drag) on each cylinder were measured by a piezoelectric load cell.

We also investigated the structural dynamics and the wake vortex modes of circular cylinder undergoing vortex-induced vibration (VIV), including a tethered cylinder [35], a neutrally buoyant cylinder placed in unbounded flow [36] or near a plane wall [37]. The vibrating cylinder exhibits the so-called “soft” synchronization phenomenon that vortex shedding frequency is synchronous with the structural vibration frequency. The transition from initial- to upper-branch is characterized by a switch of vortex formation mode from the classical 2S mode to the

newly-discovered $2P_0$ mode, as shown in Fig. 7.

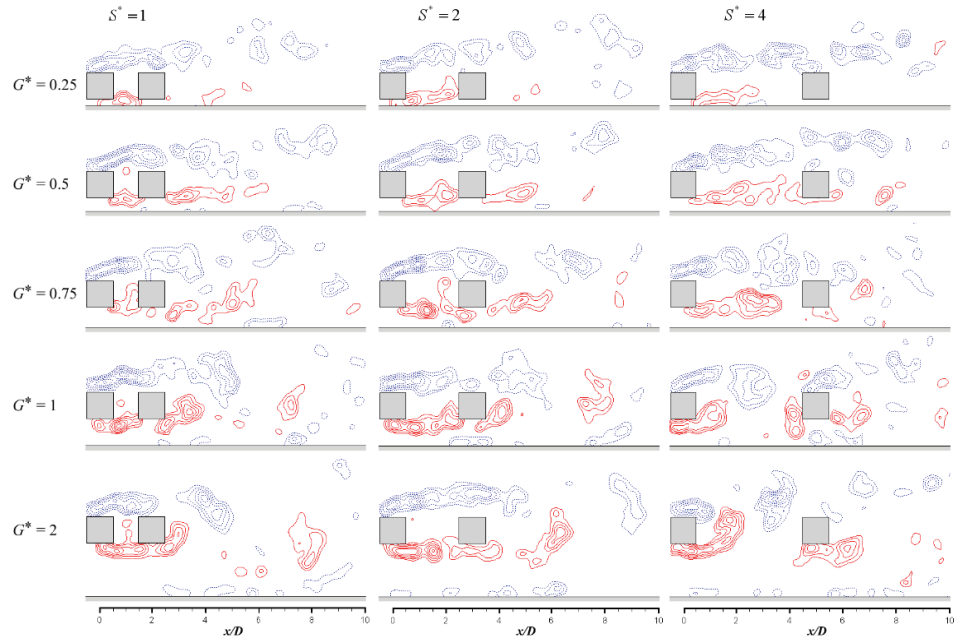


Fig. 5 2D PIV results on around two tandem square cylinders placed near a plane wall (reproduced from Wang et al. [32]): snapshot of the instantaneous normalized vorticity field at different cylinder-to-cylinder and cylinder-to-wall distance ratios. $Re = 6300$

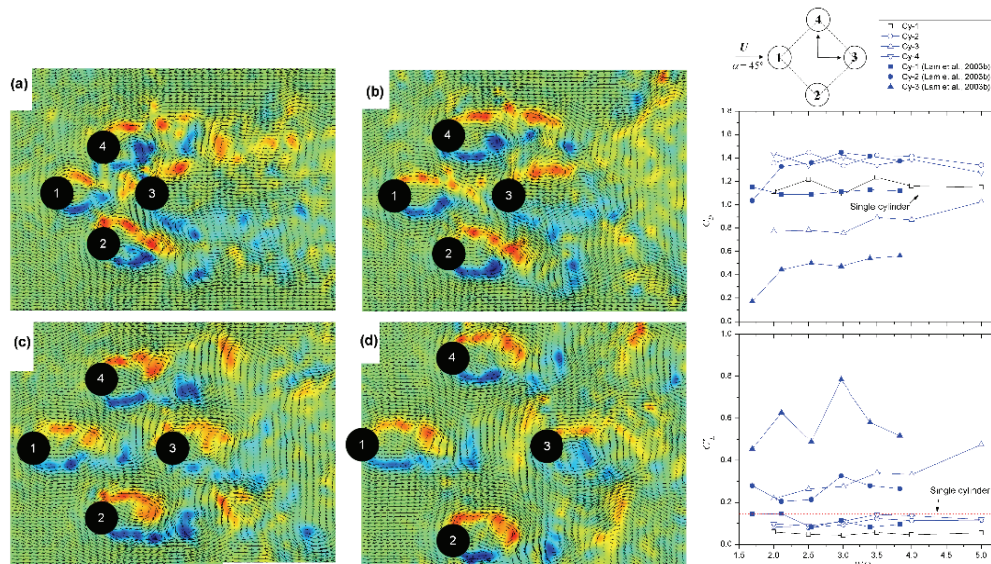


Fig. 6 2D PIV results on an array of four cylinders (reproduced from Wang et al. [34]). Left: instantaneous flow field; Right: mean drag and root-mean-square lift coefficients. $Re = 8000$

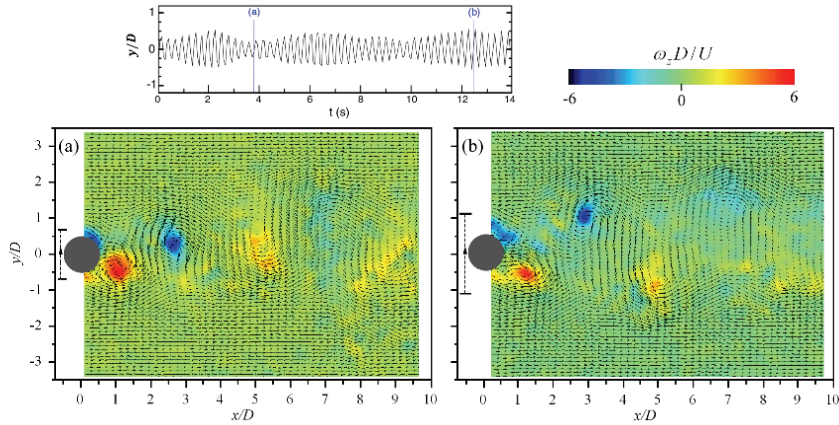


Fig. 7 2D PIV results on a cylinder undergoing VIV (reproduced from Wang et al. [36]): phase-averaged flow field at different reduced velocities. The cylinder's position and movement are highlighted, with dashed lines indicating the extent of motion. $3000 \leq \text{Re} \leq 13,000$.

Besides the above-mentioned flow configurations, we also used 2DPIV to investigate effects of cylinder rotation [38] and cylinder surface roughness pattern [39-40] for reduction of mean drag and VIV, as well as an array of multiple cylinder to simulate emergent vegetation stems [41]. In addition, stereoscopic 2D-3C PIV was used to investigate on the junction flow formed by a cylinder mounted to a flat plate. The two CCD cameras are placed at angles of $+45^\circ$ and -45° with respect to the light sheet normal, observing the illuminated area from opposite sides of the channel. The optical access is achieved through two water prisms placed on the wall of the enclosure in order to minimize the optical aberrations, see Fig. 8. The optical configuration satisfies the Scheimpflug condition, so the full viewing area is in focus. The secondary vortices in the cross-sectional plane behind the cylinder are clearly revealed.

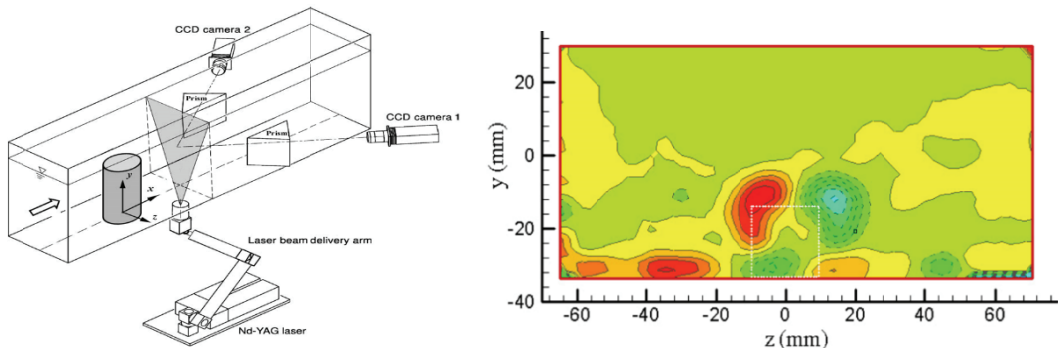


Fig. 8 2D-3C PIV results on the junction flow formed by wall-mounted cylinder: contours of secondary vortices in the cross-sectional plane. $\text{Re} = 10,000$

In the literature, 3D tomographic PIV has been applied to measure the wake flow behind cylinder, for example in air by Elsinga et al. [24] and in water by Scarano & Poelma [42], as shown in Fig. 9. The results clearly show the presence and interaction of Kármán vortex street and counter-rotating stream-wise vortex pairs. Note that Reynolds numbers in these studies are still relatively low, at $Re \sim O(10^3)$. It is envisaged that with technology development, it will soon be applicable in higher-Re flows. Actually, this technique has become more and more applied to most flow configurations that can be characterized by single-point or planar techniques, including jets and wakes, biological and biomedical flows, wall-bounded turbulence (see the latest review [6]).

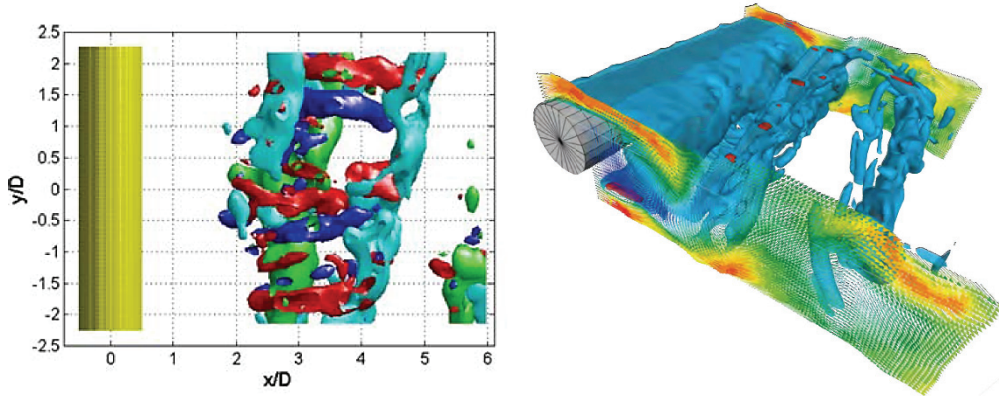


Fig. 9 3D-PIV results on the wake of a circular cylinder. Instantaneous vorticity and velocity fields. Left: Reproduced from Elsinga et al.^[24], $Re = 2700$ (in air); Right: Reproduced from Scarano & Poelma^[42], $Re = 180 - 5540$ (in water)

5 Concluding remarks and recommendations

This paper provides a brief review of the development of PIV and its applications in the hydrodynamics of cylindrical structures. PIV technique is rapidly developing, and the most exciting is the emergence of 4D-PIV, which will bring us yet a step closer to the fluid dynamicist's dream for direct measurement of the turbulent flow fields globally with sufficiently high spatial and temporal resolutions. While more sophisticated forms of PIV (e.g., TR-PIV, volumetric PIV) are emerging and will impact efforts to understand turbulence, one should not rush into complexity before mining the wealth of information that can be obtained using mature 2D PIV. New data reduction and post-processing techniques are required to further retrieve fluid

mechanical relevant information from the PIV data, such as velocity gradientslike vorticity fields, streamlines, body forces or even pressure fields. For implementation of PIV (even the basic 2D planar PIV), one needs to be well aware of the pros/cons of the technique and to follow the best-practice guidelines for the system operating in optimization to ensure the obtained results to be valid and accurate. It is recommended to combine PIV with other measurement techniques (e.g. LIF, pressure or force measurement) or numerical simulations to gain more insight into the flow field and the fluid-structure interactions.

References

1. Adrian R.I. Scattering particle characteristics and their effect on pulsed laser measurements of fluid flow: speckle velocimetry vs. particle image velocimetry. *Applied Optics*, 1984, 23(11): 1690-1691.
2. Westerweel J., Elsinga G.E., Adrian R.J. Particle image velocimetry for complex and turbulent flows. *Annual Review of Fluid Mechanics*, 2013, 45: 409-436.
3. Adrian R.J. Particle-imaging techniques for experimental fluid mechanics. *Annual Review of Fluid Mechanics*, 1991, 23(1): 261-304.
4. Adrian R.J. Twenty years of particle image velocimetry. *Experiments in Fluids*, 2005, 39(2): 159-169.
5. Scarano F. Tomographic PIV: Principles and practice. *Measurement Science and Technology*, 2013, 24(1), 012001.
6. Discretti S., Coletti F. Volumetric velocimetry for fluid flows. *Measurement Science and Technology*, 2018, 29(4): 042001.
7. Raffel M., Willert C., Kompenhans J. *Particle Image Velocimetry: A Practical Guide*. Springer, 1998.
8. Adrian R.J., Westerweel J. *Particle Image Velocimetry*. Cambridge, UK: Cambridge Univ. Press, 2011.
9. DaVis Flowmaster Software, LaVision GmbH Users Manual, 2005.
10. Hain R., Kähler C.J., Tropea C. Comparison of CCD, CMOS and intensified cameras. *Experiments in Fluids*, 2007, 42(3): 403-411.
11. Nezu I., Sanjou M. PIV and PTV measurements in hydro-sciences with focus on turbulent open-channel flows. *Journal of Hydro-Environment Research*, 2011, 5(4): 215-230.
12. Lindken R., Merzkirch W. A novel PIV technique for measurements in multiphase flows and its application to two-phase bubbly flows. *Experiments in Fluids*, 2002, 33(6): 814-825.
13. Prasad A.K. Stereoscopic particle image velocimetry. *Experiments in Fluids*, 2000, 29(2): 103-116.
14. Kähler C.J. Investigation of the spatio-temporal flow structure in the buffer region of a turbulent boundary layer by means of multiplane stereo PIV. *Experiments in Fluids*, 2004, 36(1): 114-130.
15. Nauen J.C., Lauder G.V. Quantification of the wake of rainbow trout (*Oncorhynchus mykiss*) using

- three-dimensional stereoscopic digital particle image velocimetry. *Journal of Experimental Biology*, 2002,205(21): 3271-3279.
- 16. Hori T., Sakakibara J. High-speed scanning stereoscopic PIV for 3D vorticity measurement in liquids. *Measurement Science and Technology*, 2004, 15(6): 1067-1078.
 - 17. van Doorne C.W.H., Westerweel J. Measurement of laminar, transitional and turbulent pipe flow using Stereoscopic-PIV. *Experiments in Fluids*, 2007,42(2): 259-279.
 - 18. Dennis D.J.C., Nickels T.B. Experimental measurement of large-scale three-dimensional structures in a turbulent boundary layer. Part 2. Long structures. *Journal of Fluid Mechanics*, 2011,673: 218-244.
 - 19. Beresh S.J., Henfling J.F., Spillers R.W.,et al. 'Postage-stamp PIV': Small velocity fields at 400 kHz for turbulence spectra measurements. *Measurement Science and Technology*, 2018, 29(3):034011.
 - 20. Delnoij E., Westerweel J., Deen N.G., et al. Ensemble correlation PIV applied to bubble plumes rising in a bubble column. *Chemical Engineering Science*, 1999, 54(21): 5159-5171.
 - 21. Meinhart C.D., Wereley S.T., Santiago J.G. A piv algorithm for estimating time-averaged velocity fields. *Journal of Fluids Engineering*, 2000,122(2): 285-289.
 - 22. Kähler C.J., Scholz U., Ortmanns J. Wall-shear-stress and near-wall turbulence measurements up to single pixel resolution by means of long-distance micro-PIV. *Experiments in Fluids*, 2006, 41(2): 327-341.
 - 23. Jeon Y.J., Chatellier L., David L. Fluid trajectory evaluation based on an ensemble-averaged cross-correlation in time-resolved PIV. *Experiments in Fluids*, 2014,55(7): 1766.
 - 24. Elsinga G.E., Scarano F., Wieneke B., et al. Tomographic particle image velocimetry. *Experiments in Fluids*, 2006,41(6), 933-947
 - 25. Schanz D., Gesemann S., Schröder A., et al. Non-uniform optical transfer functions in particle imaging: Calibration and application to tomographic reconstruction. *Measurement Science and Technology*, 2013, 24(2): 024009.
 - 26. Wieneke B. Volume self-calibration for 3D particle image velocimetry. *Experiments in Fluids*, 2008,45(4): 549-556.
 - 27. van Oudheusden B.W. PIV-based pressure measurement. *Measurement Science and Technology*, 2013, 24(3): 032001.
 - 28. Jeon Y.J., Gomit G., Earl T., et al. Sequential least-squarerereconstruction of instantaneous pressure field around a body from TR-PIV. *Experiments in Fluids* 2018, 59(2):27.
 - 29. Violato D., Scarano F. Three-dimensional vortex analysis and aeroacoustic source characterization of jet core breakdown. *Physics of Fluids*, 2013,25(1): 015112.
 - 30. Wang X.K., Tan S.K. Near-wake flow characteristics of a circular cylinder close to a wall. *Journal of Fluids and Structures*, 2008,24(5): 605-627.
 - 31. Wang X.K., Tan S.K. Comparison of flow patterns in the near wake of a circular cylinder and a square cylinder placed near a plane wall. *Ocean Engineering*, 2008,35(5-6): 458-472.
 - 32. Wang X.K., Hao Z., Zhang J.-X., et al. Flow around two tandem square cylinders near a plane wall.

- Experiments in Fluids, 2014,55(10): 1818.
- 33. Wang, X.K., Zhang, J.-X., Hao, Z., et al. Influence of wall proximity on flow around two tandem circular cylinders. Ocean Engineering, 2015, 94: 36-50.
 - 34. Wang X.K., Gong K., Liu H., et al. Flow around four cylinders arranged in a square configuration. Journal of Fluids and Structures, 2013, 43: 179-199.
 - 35. Wang X.K., Su B.Y., Tan S.K. Experimental study of vortex-induced vibrations of a tethered cylinder. Journal of Fluids and Structures, 2012, 34: 51-67.
 - 36. Wang X.K., Wang C., Li Y.L., Tan S.K. Flow patterns of a low mass-damping cylinder undergoing vortex-induced vibration: Transition from initial branch and upper branch. Applied Ocean Research, 2017, 62: 89-99
 - 37. Wang X.K., Hao Z., Tan S.K. Vortex-induced vibrations of a neutrally buoyant circular cylinder near a plane wall. Journal of Fluids and Structures, 2013, 39: 188-204.
 - 38. Wang X.K., Li Y.L., Yuan S.Q., et al. Flow past a near-wall retrograde rotating cylinder at varying rotation and gap ratios. Ocean Engineering, 2018, 156: 240-251.
 - 39. Zhou B., Wang X., Guo W., et al. Experimental study on flow past a circular cylinder with rough surface. Ocean Engineering, 2015, 10: 7-13.
 - 40. Zhou B., Li Y., Wang X., et al. Experimental study of dynamic drag and lift characteristics of dimpled cylinders. Marine Technology Society Journal, 2016, 50(1): 56-61.
 - 41. Zhao K., Cheng N.-S., Wang X., et al. Measurements of fluctuation in drag acting on rigid cylinder array in open channel flow. Journal of Hydraulic Engineering, 2014, 140(1): 48-55.
 - 42. Scarano F., Poelma C. Three-dimensional vorticity patterns of cylinder wakes Experiments in Fluids, 2009, 47(1): 69-83.

船舶三维声弹性理论及应用方法

邹明松

(中国船舶科学研究中心, 无锡, 214082, Email: zoumings@126.com)

摘要: 将带航速浮体三维水弹性力学理论^[1]与水声信道理论相结合, 发展了船舶三维声弹性理论与相应的计算方法。该理论方法在控制船舶振动噪声与提高水下声隐身性能, 进行船舶综合性能的优化设计等一系列工程问题中有广泛的应用需求与发展前景。本研究简述了船舶三维声弹性理论方法的基本内容, 及其在此基础上开发的船舶三维水弹性声学分析软件 THAFTS-Acoustic 的基本情况。同时, 介绍了部分新的研究进展, 对后续的发展和应用作了简要的展望。

关键词: 船舶; 流固耦合; 水弹性力学; 声弹性理论

1 引言

1984年诞生的浮体三维水弹性力学理论把海洋波浪环境中水面或水下航行器的耐波性分析、结构外载荷、结构强度与疲劳分析及结构振动分析融合在了一个统一的流固耦合理论基础上^[1]。经三十多年发展, 该理论拓展成了两个主要的研究分支——考察波浪激励下结构动响应的线性与非线性船舶三维水弹性理论, 和考察水中声学效应的船舶三维水弹性理论, 后者也称为船舶三维声弹性理论^[2]。如果下一个定义, 船舶声弹性力学是“研究惯性力、水中声压和结构弹性力之间相互作用现象的学科”^[3]。

在浮体三维水弹性力学理论的基础上, 自2009年以来, 经过持续努力逐步形成了一套较为完整的其内容还可以不断扩充的船舶三维声弹性理论及应用方法体系。在理论层面, 把船舶线性耐波性理论、船舶水弹性力学理论与船舶结构在水声信道环境中的振动声辐射和声散射理论融在一个统一的理论框架中, 为受水面和海底影响的舰船噪声分析和声隐身设计提供了新的理论支撑。在此基础上, 发展了双流域耦合三维声弹性分析方法、声弹性子结构分离与集成方法(SSI)、解析/数值混合子结构方法(MANS)以及消除不规则频率的虚拟阻抗封闭曲面方法(CVIS)等一系列可有效提高计算效率和精度、扩展应用范围的配套计算方法。开发出船舶三维水弹性声学分析软件(THAFTS-Acoustic)1.0版, 经过了数值算例、小模型试验、大尺度船体试验以及实船测试数据的考核验证, 已在十多个工

程项目中获得了良好应用。

船舶三维声弹性理论有其特有的内涵，主要体现在：①与经典的带航速浮体三维水弹性力学理论一脉相承；②证明了 Price-Wu 广义流固耦合界面条件在声弹性力学中的适用性；③在理论和计算方法上实现了船舶流固耦合振动、声辐射与海洋声传播的融合和统一分析。为实现复杂海洋信道环境中的船舶三维声弹性数值计算，提出了将近区和远区 Green 函数采用不同计算方法进行处理的设想，近区声弹性求解采用镜像法，远区声传播计算采用简正波方法，使得计算复杂度大为降低。基于该设想，已成功实现任意声速剖面的浅海水声信道环境中三维船舶流固耦合振动、声辐射与声传播的高效集成计算^[4]。并配套提出了变形的虚拟阻抗封闭曲面方法（CVIS- α ）^[5]，该方法既能有效地消除不规则频率，又能保持采用简单源方法进行海洋水声信道环境中三维弹性浮体远场声传播计算的天然优势。结合消除不规则频率的 CVIS- α 方法，简单源方法有望成为进行海洋水声环境中三维弹性浮体流固耦合振动、声辐射与声传播集成计算的最有效方法。

近来，作者提出了发展与应用船舶三维声弹性时域分析方法的设想^[6]，得到了国家自然科学基金项目的资助。该方法具有潜在的系列重要工程应用价值，下面简要介绍其基本内容。

2 船舶三维声弹性时域分析方法及其应用

该方法的基本思想来源于水动力学领域，与现有的声学领域不同。参考了水动力学中波浪与浮体相互作用的时域分析方法，通过卷积积分和 Fourier 变化由频域内的船舶声弹耦合广义动力学方程直接导出时域内的船舶声弹耦合广义动力学方程^[6]。

频域内的船舶三维声弹耦合广义动力学方程为：

$$\left\{ -\omega^2 [\mathbf{a} + \mathbf{A}(\omega)] + i\omega [\mathbf{b} + \mathbf{B}(\omega)] + (\mathbf{c} + \mathbf{C}) \right\} \xi(\omega) = \mathbf{G}(\omega) \quad (1)$$

其中， ω 为激励角频率， \mathbf{a} 、 \mathbf{b} 和 \mathbf{c} 分别为船体干模态广义质量、阻尼和刚度矩阵， $\mathbf{A}(\omega)$ 、 $\mathbf{B}(\omega)$ 和 \mathbf{C} 分别为干模态附连水质量、附连水阻尼和广义恢复力系数矩阵， $\xi(\omega)$ 为待求解的干模态主坐标位移列向量， $\mathbf{G}(\omega)$ 为作用在船体上的外激励力对应的干模态广义力列向量。

通过 (1) 式求解出 $\xi(\omega)$ 后，可进一步计算出频域内的船体振动响应、水中辐射声压以及辐射声功率等物理量^[2]。与 (1) 式相对应的时域内的船舶三维声弹耦合广义动力学方程为：

$$\mathbf{a}\ddot{\mathbf{q}} + \mathbf{b}\dot{\mathbf{q}} + \mathbf{c}\mathbf{q} = - \int_{-\infty}^t [\mathbf{K}(t-\tau)]\dot{\mathbf{q}}(\tau)d\tau + \mathbf{G}(t) \quad (2)$$

其中， $\ddot{\mathbf{q}}$ 、 $\dot{\mathbf{q}}$ 和 \mathbf{q} 分别为船体干模态对应的广义加速度、速度和位移列向量。迟滞函数矩

阵的计算公式为：

$$\begin{cases} \mathbf{K}(t) = -\frac{2}{\pi} \int_0^\infty \omega [\mathbf{A}(\omega)] \sin \omega t d\omega & t > 0 \\ \mathbf{K}(t) = 2\mathbf{B}(\infty)\delta(t) & t = 0 \end{cases} \quad (3)$$

水中实时辐射声功率的计算公式为：

$$P(\omega) = \frac{1}{T_2 - T_1} \operatorname{Re} \left[\sum_{r=1}^m \sum_{k=1}^m i\omega \eta_r B_{rk} (i\omega \eta_k)^* \right] \quad (4)$$

其中， η_r 是通过时频分析方法（如短时 Fourier 变化）得到的干模态主坐标位移响应频谱， B_{rk} 为干模态附连水阻尼元素。

船舶三维声弹性时域分析方法的主要优点在于：无需直接计算时域声场，可实时计算出船体振动响应和水中辐射声功率；计算复杂度大幅降低，计算效率大幅提高。该时域分析方法可应用于解决瞬态振动噪声问题以及与非线性因素相关联的声弹性问题。

此外，船舶三维声弹性时域分析方法还有一个重要的潜在应用，即与当前较成熟的计算流体力学方法相结合，实现流激结构振动声辐射的实时计算，实现结构振动与流场运动的耦合求解。与国家超算系统结合起来，实现流固声耦合大规模、高精度的仿真计算，解决重要工程问题。

3 小结

船舶三维声弹性理论及应用技术的发展，是以工程需求为牵引，致力于将力学理论方法应用于解决船舶与海洋工程领域中的技术问题。将持续并吸引更多的研究者在船舶三维声弹性频域分析理论及应用方法、海洋信道环境中的船舶三维声弹性理论与应用方法、船舶三维声弹性时域分析理论及应用方法、紧密结合国家超算的船舶三维水弹性声学分析高性能应用软件系统、工程应用与拓展等多个方面开展研究工作，构建研究与应用协调发展的良性体系。

致 谢

衷心感谢国家重点研发计划项目（2017YFB0202701），国家自然科学基金项目（11772304、51709241），江苏省自然科学基金项目（BK20170216）的支持。

参 考 文 献

- 1 Wu Y S. Hydroelasticity of floating bodies [PhD Thesis]. London: Brunel University, 1984.
- 2 邹明松. 船舶三维声弹性理论 [博士学位论文]. 无锡: 中国船舶科学研究中心, 2014.
- 3 邹明松, 吴有生. 船舶声弹性力学理论及其应用. 力学进展, 2017, 47: 385-428.
- 4 Jiang L W, Zou M S, Huang H, Feng X L. Integrated calculation method of acoustic radiation and propagation for floating bodies in shallow water. J. Acoust. Soc. Am., 2018, 143(5): EL430-EL436.
- 5 Zou M S, Jiang L W, Liu S X. A transformation of the CVIS method to eliminate the irregular frequency. Engineering Analysis with Boundary Elements, 2018, 91: 7-13.
- 6 Zou M S, Wu Y S, Sima C, Liu S X. A time domain three-dimensional sono-elastic method for ships' vibration and acoustic radiation analysis in water. Journal of Hydrodynamics, 2018, to be published.

Three-dimensional sono-elasticity theory of ships with applications

ZOU Ming-song

(China Ship Scientific Research Center, Wuxi, 214082.

Email: zoumings@126.com)

Abstract: The three-dimensional (3-D) linear hydroelasticity theory^[1] for traveling ships is incorporated with the hydro-acoustic channel theory to gain a three-dimensional (3-D) sono-elasticity theory of ships as well as the accompanying computational techniques. The 3-D sono-elasticity theory of ships is promising in the study of a series of engineering problems including ship vibration and noise control, improvement of the acoustic stealth of underwater vehicles, and optimization design of the overall performance of ships. In this work, the basics of the 3-D sono-elasticity theory as well as the software, THAFTS-Acoustic, are briefly introduced. Recent progress as well as an outlook of the future development and application of the 3-D sono-elasticity theory is also summarized.

Key words: Ship; Fluid-Structure interaction; Hydroelasticity; Sono-elasticity.